Applied Catalysis B: Environmental 199 (2016) 170–186

Contents lists available at ScienceDirect

Applied Catalysis B: Environmental

journal homepage: www.elsevier.com/locate/apcatb

Magnetic carbon xerogels for the catalytic wet peroxide oxidation of sulfamethoxazole in environmentally relevant water matrices

Rui S. Ribeiro[a], Zacharias Frontistis[b], Dionissios Mantzavinos[b], Danae Venieri[c], Maria Antonopoulou[d], Ioannis Konstantinou[e], Adrián M.T. Silva[f], Joaquim L. Faria[f], Helder T. Gomes[a,*]

[a] Laboratory of Separation and Reaction Engineering—Laboratory of Catalysis and Materials (LSRE-LCM), Departamento de Tecnologia Química e Biológica, Escola Superior de Tecnologia e Gestão, Instituto Politécnico de Bragança, Campus de Santa Apolónia, 5300-253 Bragança, Portugal
[b] Department of Chemical Engineering, University of Patras, Caratheodory 1, University Campus, GR-26504 Patras, Greece
[c] School of Environmental Engineering, Technical University of Crete, GR-73100 Chania, Greece
[d] Department of Environmental and Natural Resources Management, University of Patras, 2 Seferi St., GR-30100 Agrinio, Greece
[e] Department of Chemistry, University of Ioannina, GR-45110 Ioannina, Greece
[f] Laboratory of Separation and Reaction Engineering—Laboratory of Catalysis and Materials (LSRE-LCM), Faculdade de Engenharia, Universidade do Porto, Rua Dr. Roberto Frias, 4200-465 Porto, Portugal

ARTICLE INFO

Article history:
Received 6 April 2016
Received in revised form 3 June 2016
Accepted 6 June 2016
Available online 7 June 2016

Keywords:
Heterogeneous Fenton process;
Catalytic wet peroxide oxidation (CWPO)
Magnetic carbon composites
Micropollutants
Environmentally relevant water matrices

ABSTRACT

Novel magnetic carbon xerogels consisting of interconnected carbon microspheres with iron and/or cobalt microparticles embedded in their structure were developed by a simple route. As inferred from the characterization data, materials with distinctive properties may be directly obtained upon inclusion of iron and/or cobalt precursors during the sol-gel polymerization of resorcinol and formaldehyde, followed by thermal annealing. The unique properties of these magnetic carbon xerogels were explored in the catalytic wet peroxide oxidation (CWPO) of an antimicrobial agent typically found throughout the urban water cycle – sulfamethoxazole (SMX).

A clear synergistic effect arises from the inclusion of cobalt and iron in carbon xerogels (CX/CoFe), the resulting magnetic material revealing a better performance in the CWPO of SMX at the ppb level ($500\ \mu g\ L^{-1}$) when compared to that of monometallic carbon xerogels containing only iron or cobalt. This effect was ascribed to the increased accessibility of highly active iron species promoted by the simultaneous incorporation of cobalt.

The performance of the CWPO process in the presence of CX/CoFe was also evaluated in environmentally relevant water matrices, namely in drinking water and secondary treated wastewater, considered in addition to ultrapure water. It was found that the performance decreases when applied to more complex water and wastewater samples. Nevertheless, the ability of the CWPO technology for the elimination of SMX in secondary treated wastewater was unequivocally shown, with 96.8% of its initial content being removed after 6 h of reaction in the presence of CX/CoFe, at atmospheric pressure, room temperature ($T = 25\ ^{\circ}C$), pH = 3, $[H_2O_2]_0 = 500\ mg\ L^{-1}$ and catalyst load = $80\ mg\ L^{-1}$. A similar performance (97.8% SMX removal) is obtained in 30 min when the reaction temperature is slightly increased up to 60 °C in an ultrapure water matrix. Synthetic water containing humic acid, bicarbonate, sulphate or chloride, was also tested. The results suggest the scavenging effect of the different anions considered, as well as the negative impact of dissolved organic matter typically found in secondary treated wastewater, as simulated by the presence of humic acid.

An in-situ magnetic separation procedure was applied for catalyst recovery and re-use during reusability cycles performed to mimic real-scale applications. CWPO runs performed with increased SMX

* Corresponding author at: Laboratory of Separation and Reaction Engineering—Laboratory of Catalysis and Materials (LSRE-LCM), Departamento de Tecnologia Química e Biológica, Escola Superior de Tecnologia e Gestão, Instituto Politécnico de Bragança, Campus de Santa Apolónia, Bragança 5300-253, Portugal.
E-mail address: htgomes@ipb.pt (H.T. Gomes).

http://dx.doi.org/10.1016/j.apcatb.2016.06.021

concentration (10 mg L^{-1}), under a water treatment process intensification approach, allowed to evaluate the mineralization levels obtained, the antimicrobial activity of the treated water, and to propose a degradation mechanism for the CWPO of SMX.

1. Introduction

The increasing scarcity of clean water sources is driving several communities towards the reuse of treated wastewater, mainly for non-potable applications such as surface and groundwater replenishment, or agricultural and landscape irrigation – a practice already stablished as an important component of sustainable wastewater management practices [1]. Recent improvements in several analytical techniques allowed the identification and quantification of an increasing number of micropollutants present in treated wastewaters – also known as contaminants of emerging concern (CEC) [2]. Among these, the antibiotics present in treated wastewaters and their subsequent release into the environment has been receiving particular attention from the scientific community, mainly due to major public health concerns about the development of antibiotic resistant bacteria and/or resistance genes (ARB&ARG) [3].

Conventionally treated wastewaters are often considered as one of the most important anthropogenic sources of antibiotics and ARB&ARG release into the environment [4–7]. Therefore, the development of efficient and economically viable advanced treatment technologies is presently of high priority in the policy agendas of European Union member states and many other countries around the world [1,8,9], as recently suggested by a National strategy in the United States [10] and by the European COST Action ES1403 (New and emerging challenges and opportunities in wastewater reuse – NEREUS) [11]. These technologies should be able to reduce the propagation of microcontaminants typically present in treated wastewaters (such as antibiotics), usually associated with the development of ARB&ARG in the urban water cycles, and to allow the reuse of treated wastewaters as reliable alternative water sources.

Among the currently available advanced treatment technologies, the so-called Advanced Oxidation Processes (AOP) have already been shown to have superior performance in the removal of micropollutants, when compared to conventional treatments [12]. AOP have been defined by Glaze et al. in 1987 [13] as "those which involve the generation of hydroxyl radicals in sufficient quantity to affect water purification". Under this context, catalytic wet peroxide oxidation (CWPO) appears as an interesting and low cost AOP technology, characterized by its operation with simple equipment under mild conditions (typically at atmospheric pressure and low temperatures) [14,15]. CWPO relies on the transference of electrons from a suitable catalyst to hydrogen peroxide (H_2O_2) molecules, in order to promote their decomposition through the reduction of H_2O_2 to hydroxide ions (OH^-) and hydroxyl radicals ($HO^\bullet$) – a very powerful and effective oxidant for the destruction of a huge range of organic pollutants [16,17].

The well-known Fenton process is a particular case of CWPO, characterized by the generation of $HO^\bullet$ from the reaction between homogeneous Fe^{2+} and H_2O_2 under strong acidic conditions [18,19]. Nevertheless, the use of homogeneous Fe^{2+} frequently leads to the need for a complicated final chemical and physically-driven separation step for the recovery or elimination of the Fe^{2+}/Fe^{3+} ions, often found in amounts exceeding the limits allowed by common EU Directives for treated water to be discharged into natural receiving water bodies (2 mg L^{-1}). A tentative solution to overcome the typical drawbacks of the Fenton process is the immobilization of the active phase at the surface of a suitable support. Bearing this in mind, very distinct materials such as alumina, silica, mesoporous molecular sieves, zeolites, pillared clays, ion-exchange resins and nanometric diamonds have been used to support transition metals, mainly iron [17,20–28]. However, this solution frequently leads to catalysts with limited stability, mainly due to the leaching phenomenon [20,29,30]. At the same time, carbon materials with easily tuned properties, such as activated carbons [31], graphite [32], carbon nanotubes [33], carbon blacks [34], carbon aerogels [35], activated carbon xerogels [36], glycerol-based carbon materials [37] and graphene-based materials [38], have been reported as active and efficient catalysts for CWPO, although with lower performances when compared to metal-based catalysts [39]. More recently, the improved catalytic performance of highly stable carbon-based composites containing active metallic materials within their carbonaceous structure has been shown and reported as the next step in the evolution of catalysts for CWPO [39].

In the light of these findings, the ability of CWPO for the elimination of persistent microcontaminants typically present in urban wastewaters was evaluated using a set of novel magnetic carbon xerogels, consisting of interconnected carbon microspheres with iron and/or cobalt microparticles embedded in their structure. In this way, the unique electrochemical properties typically yielded by this type of carbon microstructures [40,41] are explored for the first time in CWPO, together with the high catalytic activity of iron species. Sulfamethoxazole (SMX) – an antimicrobial agent associated to the development of ARB&ARG [6] and typically found throughout the urban water cycle (in raw and in conventionally treated wastewaters [12], in raw and in conventionally treated drinking waters [42], or in surface and groundwaters [2]), was used as model of persistent micropollutant at the ppb level (500 μg L^{-1}). In addition to ultrapure water and other synthetic waters, environmentally relevant water matrices were also considered, namely drinking water and secondary treated wastewater. CWPO runs performed with increased SMX concentration (10 mg L^{-1}), under a water treatment process intensification approach, allowed to evaluate (i) the mineralization levels and (ii) the antimicrobial activity of the treated water, as well as (iii) the identification of intermediates from SMX mineralization and (iv) the proposal of a reaction mechanism for the CWPO of SMX.

2. Materials and methods

2.1. Chemicals

Sulfamethoxazole, SMX ($C_{10}H_{11}N_3O_3S$, *Mr* 253.278, analytical standard) [CAS number: 723-46-6], was purchased from Sigma-Aldrich. Acetic acid (99.8 wt.%), acetonitrile (99.9 wt.%), humic acid (technical grade), hydrogen peroxide (30 wt.%), iron(II) sulphate heptahydrate (99 wt.%), sodium bicarbonate (99.7 wt.%), sodium chloride (99.8 wt.%), sodium hydroxide (98 wt.%), sodium sulphate (99 wt.%), sodium sulphite (98 wt.%) and sulphuric acid (95 wt.%) were also obtained from Sigma-Aldrich. Methanol (99.9 wt.%) and *tert*-butanol (99 wt.%) were purchased from Fluka. Resorcinol (99 wt.%) and cobalt(II) chloride hexahydrate (99 wt.%) were

obtained from Fisher Chemical. Formaldehyde solution (37 wt.% in water, stabilized with 15 wt.% methanol) and iron(III) chloride hexahydrate (97 wt.%) were purchased from Panreac. Ascorbic acid (99 wt.%), 1,10-phenantroline (99 wt.%) and ammonium acetate (98 wt.%) were purchased from Chem-Lab NV, Serva and Penta Chemicals, respectively.

All chemicals were used as received, without further purification. Ultrapure water was used throughout the work.

2.2. Water matrices

SMX solutions were prepared in (i) ultrapure water (pH = 6.5; 0.056 mS cm^{-1} conductivity); (ii) secondary treated wastewater (pH = 7.9; 6.2 mg L^{-1} total organic carbon; 1.07 mg L^{-1} total suspended solids; 18.9 mg L^{-1} chemical oxygen demand; 311 mS cm^{-1} conductivity; 30 mg L^{-1} sulphates; 0.44 mg L^{-1} chlorides) collected from the wastewater treatment plant of the University of Patras, Greece; and (iii) drinking water (pH = 7.5; 396 mS cm^{-1} conductivity; 211 mg L^{-1} bicarbonates; 15 mg L^{-1} sulphates; 9.8 mg L^{-1} chlorides) obtained from a bottle of the commercially available brand Avra®, Greece.

Six additional synthetic water matrices were used to prepare SMX solutions, namely ultrapure water in the presence of (i) humic acid (10 mg L^{-1}); (ii) sodium bicarbonate (500 mg L^{-1} bicarbonates); (iii) humic acid (10 mg L^{-1}) and sodium bicarbonate (500 mg L^{-1} bicarbonates); (iv) humic acid (40 mg L^{-1}); (v) sodium chloride (200 mg L^{-1} chlorides); and (vi) sodium sulphate (60 mg L^{-1} sulphates).

2.3. Synthesis of carbon xerogel materials

A carbon xerogel (CX) was prepared by polycondensation of resorcinol with formaldehyde (with a molar ratio of 1:2), following the procedure described elsewhere [43]: 9.91 g of resorcinol was dissolved in 18.8 mL of distilled water, 13.5 mL of formaldehyde solution being then added and the pH adjusted to 6.1 by means of NaOH solutions (1 mol L^{-1} and 0.02 mol L^{-1}). The gelation step was allowed to proceed freely, without catalyst, in a 100 mL beaker at 85 °C during 3 days, the recovered gel being grounded (particle sizes in the range 0.106–0.250 mm), dried in oven (from 60 to 150 °C, defining a heating ramp of 20 °C day^{-1}) and annealed under a N_2 flow (100 cm^3 min^{-1}) in a tubular vertical oven, at 120 °C, 400 °C and 600 °C during 60 min at each temperature, and then at 800 °C for 240 min, defining a heating ramp of 2 °C min^{-1}, resulting in CX materials. CX/Fe was synthesized using the same procedure, except that iron(III) chloride hexahydrate was added to the resorcinol solution (considering a Fe/resorcinol molar ratio of 0.05) prior to formaldehyde, being then stirred in an orbital shaker (160 rpm) during 2 h. Likewise, CX/Co was obtained by adding cobalt(II) chloride hexahydrate (considering a Co/resorcinol molar ratio of 0.025). CX/CoFe was obtained by adding iron(III) chloride hexahydrate (considering a Fe/resorcinol molar ratio of 0.05) and cobalt(II) chloride hexahydrate (considering a Fe/Co molar ratio of 2 as previously reported for iron-copper bimetallic nanoparticles embedded within ordered mesoporous carbon composite catalysts [44]).

Prior to their use, the magnetic carbon xerogels were washed with 1 L of a HCl solution (pH = 3) at 50 °C and dried overnight at 60 °C. This final step aims to wash out from the material metal species that are not strongly embedded in the carbonaceous structure of the magnetic carbon xerogels, in this way increasing the stability of the catalysts synthesized and limiting the contamination of the treated waters during the CWPO process.

2.4. Characterization techniques

The textural properties of the carbon xerogel materials were determined from N_2 adsorption–desorption isotherms at −196 °C, obtained in a Quantachrome NOVA 4200e adsorption analyser. Before the analysis, all samples were outgassed for 6 h at 130 °C. The specific surface area (S_{BET}) was determined by applying the Brunauer-Emmett-Teller (BET) equation [45]. The micropore volume (V_{micro}) and the non-microporous surface area (S_{meso}) were determined by the t-method using an appropriate standard isotherm [46]. The total pore volume (V_{total}) was derived from the amount of N_2 adsorbed at a relative pressure close to unity, namely at $p/p^{\circ} = 0.995$ [47]. The average pore diameter (d_{pore}) was estimated from Eq. (1), assuming that the pores are of cylindrical shape and most of the surface area arises from the inner walls of the pores [48].

$$d_{pore} = \frac{4V_{total}}{S_{BET}} \quad (1)$$

The pH at the point of zero charge (pH_{PZC}) of the materials was determined adapting the methodology described elsewhere [49]. Briefly, solutions with varying initial pH (2–11) were prepared using HCl (1.0 mol L^{-1}) or NaOH (1.0 mol L^{-1}) and 20 mL of NaCl (0.01 mol L^{-1}) as electrolyte. Each solution was contacted with 0.05 g of the material and the final pH was measured after 48 h of continuous stirring at room temperature. The pH_{PZC} was determined by intercepting the obtained final pH vs. initial pH curve with the straight line final pH = initial pH [50,51].

X-ray photoelectron spectroscopy (XPS) analysis was performed in a Kratos Axis Ultra HAS using a monochromatic Al X-ray source (1486.7 eV), powered at 15 kV (90 W), in lens hybrid mode. For the data analysis the charge correction was based on the C 1s peak (285 eV). After a Shirley background subtraction, the peaks were fitted to Gaussian curves using the CasaXPS software.

X-ray diffraction (XRD) analysis was performed in a PANalytical X'Pert MPD equipped with a X'Celerator detector and secondary monochromator (Cu Kα, λ = 0.154 nm; data recorded at a 0.017° step size). Highscore Plus software was used to identify the crystallographic phases present in the XRD diffraction patterns.

Scanning electron microscopy (SEM) images in secondary electron (SE) and backscattered electron (BSE) detection modes were obtained using a FEI Quanta 400FEG ESEM/EDAX Genesis X4M instrument equipped with an Energy Dispersive Spectrometer (EDS). At least 110 counts were performed by using ImageJ software in order to estimate the size of the primary carbon microspheres of the carbon xerogel materials; likewise, at least 65 counts were performed in order to estimate the size of the metal particles embedded in their structure.

The content of Fe and Co in the carbon xerogel materials was determined by atomic absorption analysis of the solution resulting from the acidic digestion of the solids. For this purpose, each sample was initially dispersed in distilled water (1 mg mL^{-1}). 1 mL of each dispersion was later added to 1 mL of aqua regia (mixture of pure nitric acid and hydrochloric acid, with a volume ratio of 1:3), the resulting solution being heated at 60 °C for 48 h in order to promote the sample digestion. After being cooled down to room temperature, the digested samples were filtered (CA syringe filters, 0.45 mm) and the Fe and Co concentrations were determined by a PerkinElmer PinAAcle 900 atomic absorption spectrometer, using single and multi-element hollow cathode lamps (Lumina N3050126 and N3050214) for the determination of Fe and Co, respectively.

Thermogravimetric analysis (TGA) was performed using a Netzsch TG 209 F3 Tarsus equipment under oxidative atmosphere, upon heating the samples from 30 °C to 950 °C at 20 °C min^{-1}.

2.5. Catalytic wet peroxide oxidation experiments

Batch CWPO experiments were performed in a well-stirred (500 rpm) cylindrical jacketed glass reactor (internal diameter = 6 cm; height = 9.5 cm) connected to a thermostatic water bath with temperature control. The reactor was loaded with 250 mL of a SMX solution in different water matrices and, upon stabilization at the desired temperature, the solution pH was adjusted when necessary, using H_2SO_4 and NaOH solutions (1 mol L^{-1}), the experiments being then allowed to proceed freely, without further conditioning of pH. After the initial pH adjustment, the catalyst was added and a calculated volume of H_2O_2 (30 wt.%) was injected into the system, in order to reach the desired concentration, that moment being considered as t_0 = 0 min. Typical CWPO experiments were conducted during 6 h, with $[SMX]_0$ = 500 μg L^{-1}, T = 25 °C, pH = 3, $[H_2O_2]_0$ = 500 mg L^{-1} and catalyst load = 20 mg L^{-1}.

Pure adsorption runs were performed in order to assess the possible contribution of adsorption in the removal of SMX by CWPO. In this case, the amount of H_2O_2 was replaced by ultrapure water. Blank experiments, without any catalyst, were also carried out to assess possible non-catalytic oxidation promoted by H_2O_2. In order to show the role of the HO• radicals in the CWPO process, *tert*-butanol (tBuOH) – a strong HO• scavenger [13], was added before one reaction.

Selected experiments were performed in triplicate, in order to assess reproducibility and error of the experimental results. It was found that the standard deviation of the SMX determination was never superior to 3%.

In order to evaluate the stability of the CX/CoFe catalyst in the CWPO of SMX, reusability cycles were performed as depicted in Fig. 1, namely: after each run, the catalyst was separated taking advantage of its magnetic properties, just by allowing its deposition on the magnetic stirring bar. Afterwards, the treated water was recovered, and the catalyst was reused in CWPO upon the addition of a fresh SMX solution (500 μg L^{-1}). Both ultrapure water and secondary treated wastewater were used in this study.

2.6. Analytical methods

The concentration of SMX was determined by high performance liquid chromatography (HPLC), using an Alliance HPLC system equipped with a photodiode array detector (Waters 2996), a separation module including a gradient pump (Waters 2695) for solvent delivery (0.35 mL min^{-1}) and a Kinetex C18 100A column (150 mm × 3 mm; 2.6 mm particle size) maintained at T = 45 °C. The mobile phase consisted in an isocratic method of ultrapure water (60%) and acetonitrile (40%). The SMX absorbance peaked at 270 nm, as determined from the corresponding UV–vis absorption spectrum (Waters 2996). For this purpose, small aliquots were periodically withdrawn from the reactor, and an excess of methanol – a known HO• scavenger [52,53], was immediately added in order to consume residual HO• and to instantaneously stop the reaction, the resulting samples being then placed in ice. The samples were filtered (PVDF syringe filters, 0.2 mm) prior to analysis.

Dissolved Fe content was determined by a colorimetric method with 1,10-phenantroline, according to ISO 6332 and measuring the absorbance at 510 nm [54]. Dissolved Co content was determined by a PerkinElmer PinAAcle 900 atomic absorption spectrometer using a multi-element hollow cathode lamp (Lumina N3050214). The concentration of H_2O_2 was followed by a colorimetric method, as described elsewhere [53]. Total organic carbon (TOC) was determined using a Shimadzu TOC-L CSN analyser.

The transformation by-products (TBPs) generated during the CWPO of SMX were identified by an Ultra-High Performance LC system by Thermo (Dionex Ultimate 3000 RS pump, RS Autosampler, RS column thermostat), interfaced with a microTOF Focus II – time of flight mass spectrometer (Brüker Daltonics, Germany). All electrospray ionization (ESI)-MS experiments were acquired both in positive and negative mode. The mass spectrometer part was operated using otof control software under the adopted conditions: dry gas flow rate of 8 L min^{-1} (N_2), nebulizer pressure of 2.4 bar, capillary voltage at 4500 V, end plate offset at 500 V, hexapole RF 100.0 Vpp and dry temperature at 200 °C. The chromatographic separations were run on a C18 Acclaim™ RSLC 120 column (100 mm × 2.1 mm; 2.2 mm particle size; Thermo Scientific), protected by a column guard from Waters and thermostated at T = 30 °C. Injection volume was 10 μL, while water with 0.01% formic acid (Solvent A) and methanol (Solvent B) were used as binary mobile phase mixtures. For both ionization modes the adopted elution gradient starts with 1% of methanol and increases linearly to 99% in 14 min. Initial conditions were reached in 17 min and kept constant for 1 min. The total run time for each injection was 18 min. The flow rate was kept constant at 0.2 mL min^{-1}. To ensure mass accuracy of ±5 ppm, prior to each analysis the TOF mass analyzer was externally calibrated using sodium formate, in the scan range m/z 50–1000.

2.7. Antimicrobial activity

For the determination of the antimicrobial activity the samples were treated with an excess of sodium sulphite in order to consume residual H_2O_2 [55], and the solution pH was adjusted to 7 with a NaOH solution (0.5 mol L^{-1}). The antibiotic activity against *Klebsiella pneumoniae* (Gram negative) and *Staphylococcus aureus* (Gram positive) was then used to evaluate the toxicity of the water prior and after treatment. For that purpose, initial bacterial inocula (1×10^4 CFU mL^{-1}) were incubated at 37 °C for 24 h in the presence of SMX solutions with different concentrations and with the oxidized samples, followed by optical density measurement at 630 nm, using a microplate reader (Labtech LT-4000 Plate Reader).

The bactericidal effect of the metals embedded in the magnetic carbon xerogels (i.e., Fe and Co) was assessed with the same two bacterial strains. In this case, a set of experiments was performed in the dark with 2 mg L^{-1} of Co and Fe ionic solutions, which were spiked with the bacteria of interest, at a concentration of 10^4 CFU/mL. At specific time intervals (i.e., 0, 30, 60, 120, 180 and 240 min) samples were taken and after serial dilutions were streaked onto nutrient agar plates, which were then incubated at 37 °C for 24 h. Afterwards, the bacterial density of *K. pneumoniae* and *S. aureus* was determined by colony counts.

3. Results and discussion

3.1. Materials characterization

Both CX and the magnetic carbon xerogels developed for this work were extensively characterized. The main textural properties of the carbon xerogel materials are given in Table 1. As observed, all the carbon xerogel materials have a well-developed specific surface area, with S_{BET} values in the range 510–650 m^2 g^{-1}. CX is mainly a mesoporous material, with a ratio V_{mic}/V_{total} = 0.17 and d_{pore} = 6.7 nm. However, as observed from the corresponding values of S_{meso}, the inclusion of metal species leads to a substantial decrease of the mesoporous area, the resulting magnetic carbon xerogels being mainly microporous materials. This effect is particularly pronounced when Co is incorporated, with CX/CoFe and CX/Co having a strong microporous character (V_{mic}/V_{total} = 0.68 and 0.81, respectively, and d_{pore} of ca. 2 nm).

Regarding the surface chemistry, the inclusion of metal species, in particular Fe, leads to a slight decrease in the basicity of the resulting carbon xerogel materials when compared to that of CX, as

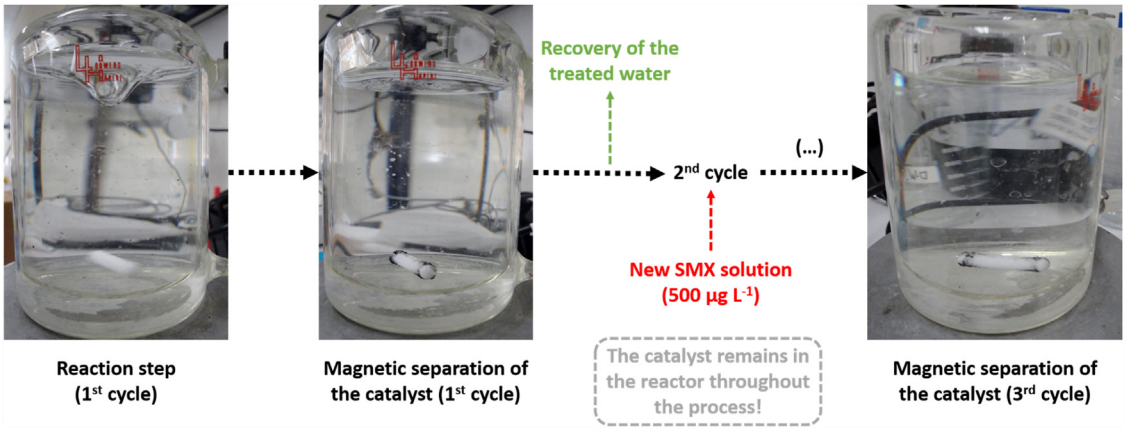

Fig. 1. Experimental procedure during the CWPO reusability cycles performed with CX/CoFe.

Table 1
Properties of the carbon xerogel materials: specific surface area (S_{BET}), non-microporous specific surface area (S_{meso}), micropore volume (V_{micro}), total pore volume (V_{total}), average pore diameter (d_{pore}), pH at the point of zero charge (pH_{PZC}) and total Fe and Co contents.

Material	Parameter								
	S_{BET} ($m^2\ g^{-1}$)	S_{meso} ($m^2\ g^{-1}$)	V_{mic} ($cm^3\ g^{-1}$)	V_{total} ($cm^3\ g^{-1}$)	V_{mic}/V_{total}	d_{pore} (nm)	pH_{PZC}	Fe (wt.%)	Co (wt.%)
CX	650	240	0.19	1.09	0.17	6.7	9.2	–	–
CX/Fe	510	90	0.17	0.46	0.37	3.6	6.6	6.5	–
CX/Co	580	30	0.23	0.28	0.82	1.9	8.3	–	0.9
CX/CoFe	530	40	0.20	0.30	0.67	2.3	7.7	4.6	2.1

observed from the corresponding values of pH_{PZC} given in Table 1. The Fe content in the bimetallic magnetic carbon xerogel (CX/CoFe) is lower than that embedded in the structure of the monometallic CX/Fe; on the opposite, a higher content of Co is observed in the bimetallic CX/CoFe when compared to the monometallic CX/Co.

The carbon xerogel materials were also analysed by SEM. As observed in Fig. 2, the morphology of the materials helps to elucidate the differences observed in the textural properties of the carbon xerogels with and without metal species embedded in their structure. Fig. 2a and e correspond to CX, a typical carbon xerogel material, composed by large particles of carbon (153 ± 51 mm, as determined from SEM measurements). This is the result of the sol-gel polycondensation of resorcinol (R) and formaldehyde (F), in which two main reactions occur: (i) addition of F to the aromatic ring of R, leading to the formation of reactive R anions and hydroxymethyl derivatives; (ii) condensation of the hydroxymethyl derivatives to form methylene and methylene ether bridged compounds [56]. The condensation products form clusters whose aggregation leads to the formation of large particles [56]. In this case, the concentration of F and R, as well as the pH, are the most important factors controlling the properties of the RF gels [56], and thus the properties of the resulting carbon xerogels after thermal annealing. On the opposite, the magnetic carbon xerogels are composed by aggregates of interconnected carbon microspheres (cf. Fig. 2b–d) with iron and/or cobalt microparticles embedded in their structure (cf. Fig. 2f–h). This observation suggests that the aggregation of clusters formed during the polycondensation of R and F is limited by both metals considered. Nevertheless, the size of the primary carbon microspheres and the size and distribution of the metal particles are different. Bearing this in mind, and since the magnetic carbon xerogels were prepared in the exactly same conditions as CX, except that iron and/or cobalt precursors were added during the sol-gel polycondensation of R and F, it can be concluded that the nature of the metal precursor affects the structure and morphology of the resulting carbon xerogel materials. As previously described elsewhere, the metal cations are expected to form bonds with the negatively charged functional groups of the RF gel, thus being able to catalyse the polymerization reaction and to influence the structure of the carbon xerogel [56].

A deeper analysis of Fig. 2b–d suggests that CX/Fe possesses the biggest and more complex aggregates of interconnected primary carbon microspheres among the magnetic carbon xerogels, whereas CX/Co is at the opposite position, with the less extended aggregates; the bimetallic CX/CoFe possesses intermediate properties when compared to the monometallic materials. In addition, it is also observed that the distribution of metal particles at the surface of the magnetic carbon xerogels is more evident in the materials with Co embedded in their structure (i.e., CX/Co and CX/CoFe). This observation is even more relevant if the content of Fe and Co in the magnetic carbon xerogels is considered. Specifically, although CX/Fe and CX/CoFe possess ca. the same total metal content (6.5% vs. 4.6% + 2.1%, i.e., 6.7%; cf. Table 1), the amount and distribution of metal particles at the surface of CX/CoFe (cf. Fig. 2d) is more visible than that observed with CX/Fe (cf. Fig. 2b).

In order to confirm the metal distribution at the surface of the magnetic carbon xerogels, these materials were also analysed by XPS. The corresponding XPS spectra and the atomic surface concentrations of C 1s, O 1s, Fe 2p and Co 2p are given in Fig. 3 and Table 2, respectively. As observed in Fig. 3, the Fe 2p and Co 2p regions in the XPS spectrum of CX/CoFe are qualitatively similar to those same regions in the XPS spectra of CX/Fe and CX/Co, respectively. However, the simultaneous incorporation of Fe and Co leads to an enhanced metal distribution at the surface of the bimetallic CX/CoFe (cf. Table 2), confirming the previous observations. In addition, if the surface weight concentrations given in Table 2 are compared to the total Fe and Co contents given in Table 1, it is suggested that some metal particles are surrounded by the organic phase during the synthesis of the monometallic CX/Fe and CX/Co catalysts, therefore being less accessible. In the opposite, when Co and Fe are simultaneously incorporated in the bimetallic CX/CoFe, the metals are preferentially located at the surface of the catalyst.

Further insights on the morphology and particle size distribution of the magnetic carbon xerogels are given in Fig. 4, in which SEM images obtained with higher magnification (Fig. 4a, c and e)

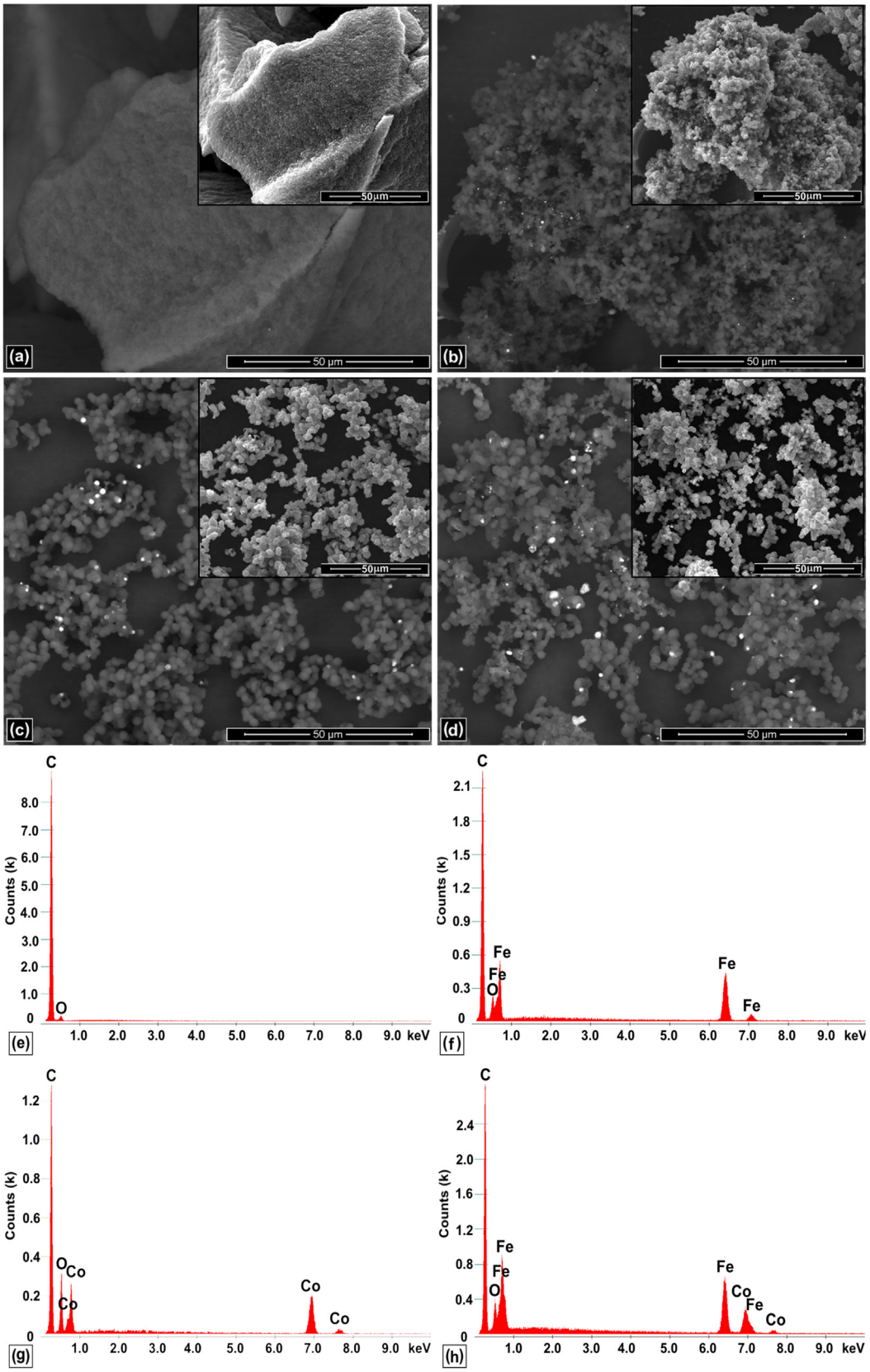

Fig. 2. SEM micrographs of (a) CX, (b) CX/Fe, (c) CX/Co and (d) CX/CoFe, obtained in (main) BSE and (inset) SE mode. EDX spectra of (e) CX, (f) CX/Fe, (g) CX/Co and (h) CX/CoFe.

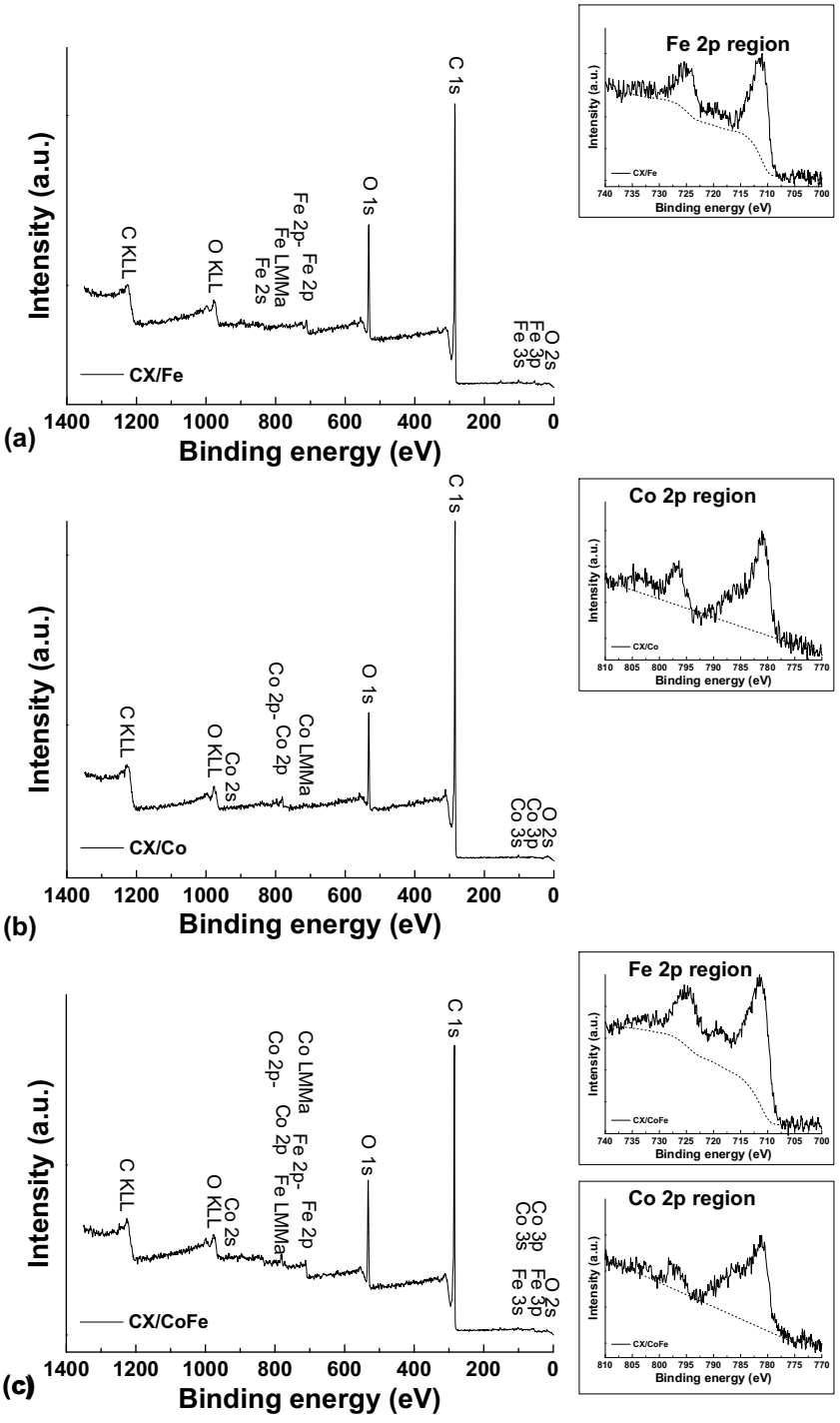

Fig. 3. XPS spectra of (a) CX/Fe, (b) CX/Co and (c) CX/CoFe. Insets: detailed XPS spectra of Fe 2p and/or Co 2p regions.

Table 2
Atomic and weight concentrations of C 1s, O 1s, Fe 2p and Co 2p, at the surface of the magnetic carbon xerogels, as determined from the XPS analysis.

Material	Atomic surface concentration (%)				Weight surface concentration (%)			
	C 1s	O 1s	Fe 2p	Co 2p	C 1s	O 1s	Fe 2p	Co 2p
CX/Fe	84.82	14.48	0.70	–	79.00	17.97	3.03	–
CX/Co	89.35	10.19	–	0.46	84.95	12.91	–	2.14
CX/CoFe	84.56	13.64	1.19	0.61	76.01	16.33	4.97	2.69

are shown. During the synthesis procedure, the metal particles are expected to be anchored to the carbon structure, thus preventing their growth [56]. This mechanism is confirmed by the small size of the metal particles observed regardless of the magnetic carbon xerogel considered. Nevertheless, as detailed in Fig. 4b, d and f, CX/Fe possesses the smallest primary carbon microspheres and

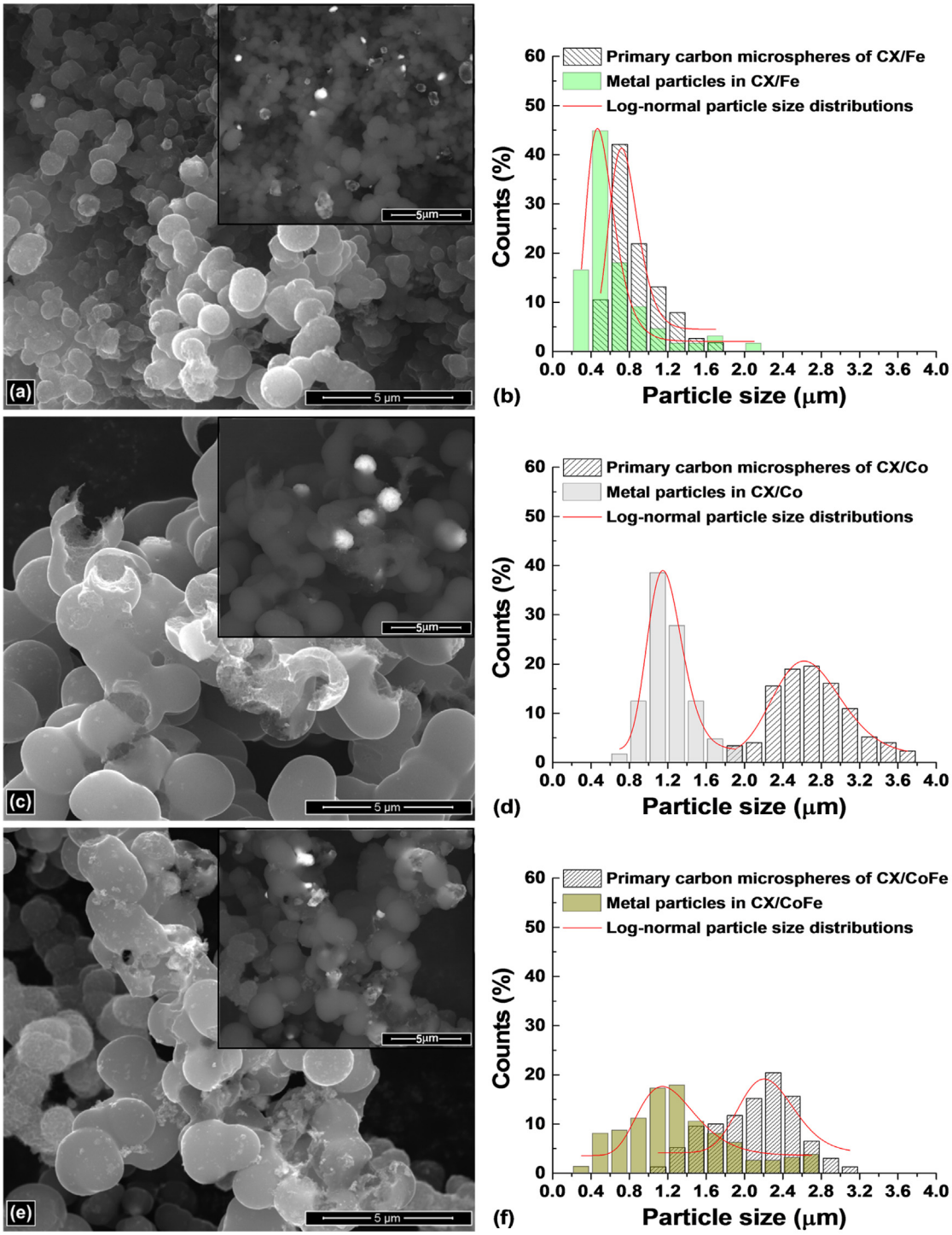

Fig. 4. SEM micrographs, obtained in (main) SE and (inset) BSE mode, and histogram of particle size distribution of (a, b) CX/Fe, (c, d) CX/Co and (d, e) CX/CoFe.

metal particles, whereas CX/Co is at the opposite position, with the biggest carbon microspheres and metal particles; once again, the bimetallic CX/CoFe possesses intermediate properties when compared to the monometallic materials.

The carbon xerogel materials were also characterized by XRD, the corresponding results being given in Fig. 5. The absence of an identifiable crystallographic phase in the diffraction pattern of CX confirms the prevalence of amorphous carbon in its composition. On the other hand, the incorporation of iron and/or cobalt during the synthesis procedure promotes the formation of graphitic (i.e., more ordered) carbon, as observed in the diffraction patterns of the magnetic carbon xerogels. Magnetite (Fe_3O_4; with a lattice parameter $a = 8.380$ Å) and iron (Fe^0; $a = 2.868$ Å) were identified in the diffraction pattern of CX/Fe, in addition to graphite. The incorporation of Co during the synthesis of CX/Co leads to the formation of cobalt (Co^0; $a = 3.544$ Å), cobalt(II, III) oxide (Co_3O_4; $a = 8.089$ Å) and cobalt(II) oxide (CoO; $a = 4.268$ Å). The simultaneous incorporation of Co and Fe leads to the formation of cobalt ferrite ($CoFe_2O_4$; $a = 8.388$ Å) and Fe^0 ($a = 2.863$ Å), in addition to graphite, as observed in the diffraction pattern of CX/CoFe.

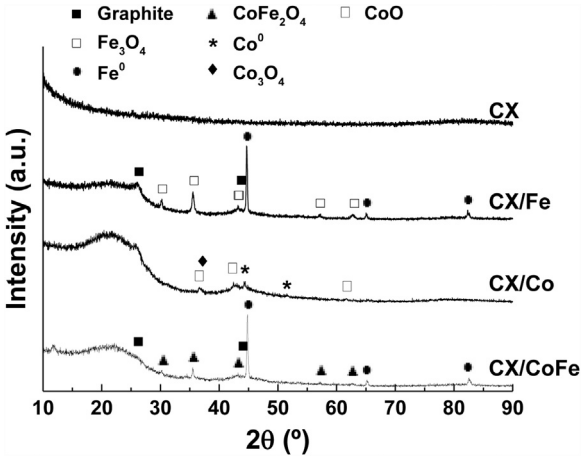

Fig. 5. XRD diffraction patterns of the carbon xerogel materials.

If the values of pH_{PZC} obtained for the magnetic carbon xerogels (cf. Table 1) are compared with those recently reported in the literature for their main metal oxide constituents [57], it is observed that they follow the same order: CX/Fe (6.6) < CX/CoFe (7.7) < CX/Co (8.3), while Fe_3O_4 (6.5) < $CoFe_2O_4$ (7.5) < CoO (9.2) and Co_3O_4 (9.4). Therefore, the pH_{PZC} of the magnetic carbon xerogels can be partially explained by the different contributions of the main metal oxides detected by XRD.

3.2. CWPO experiments

The performance of the carbon xerogel materials in the CWPO of SMX solutions at the ppb level (500 μg L^{-1}) was evaluated in screening experiments performed during 6 h at room temperature and atmospheric pressure, under the conditions described in Section 2.5. The removals of SMX obtained by pure adsorption and by CWPO are given in Fig. 6. As observed, the maximum difference of SMX removal due to H_2O_2 addition is obtained with CX/CoFe, revealing the superior performance of the hybrid magnetic carbon xerogel material with cobalt and iron microparticles embedded in its structure. It should be noted that the SMX removal obtained when using CX is similar, but in this case ascribed to adsorption of the pollutant (and not to catalytic degradation). The non-catalytic removal of SMX (i.e., with H_2O_2 but in the absence of catalyst), obtained under the same conditions (results not shown) is rather low, corresponding to ca. 13% of its initial content.

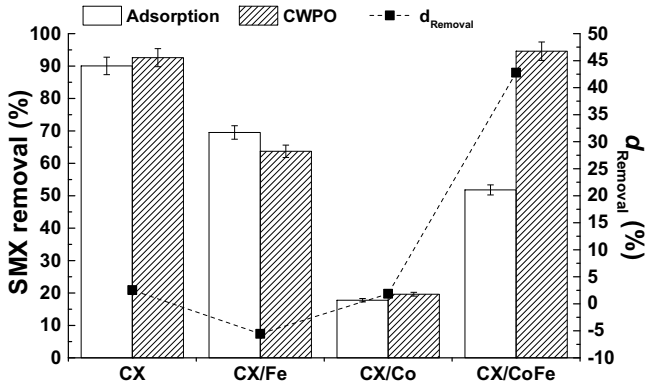

Fig. 6. Removal of SMX (500 μg L^{-1}) obtained after 6 h in adsorption and CWPO runs (bars/left axis) performed with the carbon xerogel materials (20 mg L^{-1}), and respective difference due to H_2O_2 addition [$d_{Removal}$ (squares/right axis)], at T = 25 °C, pH = 3 and, in CWPO runs, $[H_2O_2]_0$ = 500 mg L^{-1}.

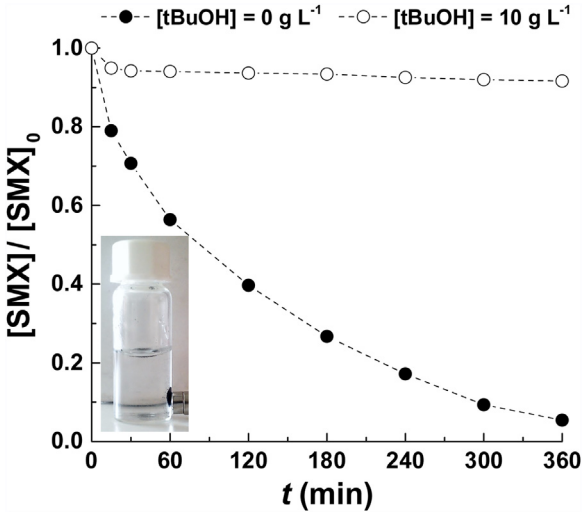

Fig. 7. Effect of *tert*-butanol (tBuOH) on the CWPO removal of SMX (500 μg L^{-1}) when using CX/CoFe under the experimental conditions of Fig. 6. Inset: magnetic separation of CX/CoFe in ultrapure water.

As observed from the difference of SMX removal due to H_2O_2 addition ($d_{Removal}$, corresponding to the increase of the pollutant removal obtained in the CWPO experiments compared to that obtained in the pure adsorption experiments) given in Fig. 6, a clear synergistic effect arises from the combination of Fe and Co in CX/CoFe, when its performance is compared to that of the monometallic catalysts (CX/Fe and CX/Co). This effect may be explained by the enhanced accessibility to the highly active Fe species existing at the surface of CX/CoFe, promoted by the simultaneous incorporation of Co, as discussed in Section 3.1.

Due to its higher performance, CX/CoFe was object of additional studies. In order to evaluate the participation of HO• radicals in the process, *tert*-butanol (tBuOH) – a strong HO• scavenger [13], was added before a CWPO experiment performed in the presence of CX/CoFe. When the SMX concentration decay curves obtained in the presence and absence of tBuOH are compared (cf. Fig. 7), it is observed that the removal of SMX is greatly suppressed by tBuOH. Although not directly supported by quantification of the HO• radicals formed during the process, this indirect result suggests the predominant role of HO• radicals in the CWPO of SMX. Therefore, the high catalytic performance of CX/CoFe in the CWPO of SMX is unequivocally highlighted by the concentration decay curves given in Fig. 7. To the best of our knowledge, this is the first time in which magnetically recoverable carbon xerogels consisting of interconnected carbon microspheres and magnetic materials are reported as active catalysts in CWPO applications.

The magnetic sensitivity of CX/CoFe (cf. inset of Fig. 7) is an additional advantage, since it can be explored for the development of in-situ magnetic separation systems. In this way, the typical separation step required in the Fenton process for the removal of dissolved Fe species in the treated water may be avoided. Nevertheless, since CX/CoFe possesses Fe and Co in its structure (cf. Table 1 and Figs. 2 and 5), this assumption should be confirmed. In this sense, the amounts of Fe and Co leached to the treated water were determined at the end of the CWPO experiment performed with CX/CoFe. The Fe leached to the treated water during this experiment was 0.1 mg L^{-1} – i.e., 20-fold below the limits allowed by common EU Directives for treated water to be discharged into natural receiving water bodies (2 mg L^{-1}) and even below the maximum limits allowed for water intended for human consumption (0.2 mg L^{-1}) [58]. Likewise, the leaching of Co was also rather low (0.2 mg L^{-1}), although in this case there is a lack of standards for

treated wastewater and even for drinking water, reflecting its minimal risk [59].

In addition, it should be noted that the experiments depicted in Fig. 7 were performed at room temperature and atmospheric pressure, putting in evidence the potential of this novel hybrid magnetic carbon xerogel material with cobalt and iron embedded in its structure for economically viable CWPO applications.

3.2.1. Individual effect of the operating parameters

In order to investigate the operating conditions that maximize the performance of SMX removal by CWPO in the presence of CX/CoFe, the individual effect of several operating parameters was evaluated, namely catalyst load, H_2O_2 dosage, SMX concentration, initial pH and temperature (cf. Fig. 8). As expected, the SMX removal increases with increasing catalyst dosage (cf. Fig. 8a). Regarding H_2O_2 dosage, although the stoichiometric amount of H_2O_2 needed to completely mineralise SMX is ca. 1.3 mg L^{-1}, it is observed that SMX removal goes through a maximum, corresponding to $[H_2O_2]_0$ = 500 mg L^{-1} (cf. Fig. 8b). The higher requirement of H_2O_2 may be explained by the operating conditions considered (mainly due to the low catalyst dosage and room temperature). In the opposite, when the H_2O_2 dosage is increased 2-fold up to 1000 mg L^{-1}, the SMX removal decreases. This observation suggests that under these conditions the formed HO• radicals may react preferably with H_2O_2, leading to non-reactive species such as H_2O and O_2 – through a series of parasitic reactions that are more significant when low pollutant concentrations are considered [60], such as some employed in the current study. In Fig. 8c is observed that SMX removal apparently decreases when the initial SMX concentration increases; however, the pollutant mass removal rate actually increases from 4.0 μg g^{-1} h^{-1} up to 10.2 μg g^{-1} h^{-1}, leading to a ca. 2.5-fold gain in the efficiency of catalyst usage after 6 h of reaction. When CWPO is carried out without adjusting the natural pH of the SMX solution (i.e., at pH = 5.9), ca. 34% of the initial pollutant is removed (cf. Fig. 8d), and only ca. 20% of the pollutant is removed when the initial pH is increased up to 9. These results suggest that the catalyst CX/CoFe can be used in the CWPO of SMX in the pH range 3–6, although it loses some catalytic activity with increasing pH. The effect of temperature was also explored. As observed in Fig. 8e, the performance of CWPO for the elimination of SMX is substantially enhanced when the temperature is slightly increased from room temperature (25 °C) up to mild temperatures (40–60 °C). This effect is particularly observed at T = 60 °C, with SMX being almost completely removed in 30 min.

The kinetics of SMX removal by CWPO in the presence of CX/CoFe were further explored through the determination of apparent first order reaction rate constants (k_{app}) for all the experiments depicted in Fig. 8. The results obtained are shown in Fig. 9a. The majority of the experimental data are well described by the kinetic model considered, the results confirming the trends suggested by the SMX concentration decay curves shown in Fig. 8. However, it should be noted that this is a pseudo first order kinetic model relative to SMX concentration. Therefore, the effect of other contributions (mainly H_2O_2 dosage and catalyst concentration) is not accounted in the model. In addition, it is well known that the rate of advanced oxidation of organic contaminants depends on the substrate concentration. Usually the reaction obeys to a first order rate expression with respect to the substrate concentration at low concentrations, but it shifts towards zero order at higher concentrations [61]. This behaviour can be explained taking into account the rate-limiting step, where the reactive oxidizing species (mainly HO• radicals) become the limiting factor for the reaction. This might explains why k_{app} changes by changing the initial SMX concentration, while maintaining constant the initial values of the other operating parameters. In order to better understand the effect of temperature on the reaction rates, the Arrhenius plot (cf. Fig. 9b) was used to determine the apparent activation energy (E_a), a value of E_a = 69.8 kJ mol^{-1} being obtained.

3.2.2. Environmentally relevant water matrices

Ultrapure water may be considered an attractive matrix to conduct studies for the initial design and evaluation of advanced treatment technologies, mainly due to its ease of manipulation, simplicity and reproducibility of the experimental results. However, antimicrobial agents like SMX are typically released into the environment in much more complex water matrices, like conventionally treated wastewater [12]. Furthermore, SMX has also been found in drinking water [42], raising serious public health concerns. These environmentally relevant water matrices, in particular the treated wastewater, contain multiple natural and anthropogenic compounds [3], increasing their complexity and hindering the performance of treatment technologies. Bearing this in mind, the influence of the water matrix on the performance of SMX removal by CWPO was assessed in this work, using secondary treated wastewater and drinking water (cf. Section 2.2) spiked with SMX at the ppb level (500 μg L^{-1}). The results obtained are shown in Fig. 10a. As observed, the SMX removal decreases with the increasing complexity of the water matrix. Specifically, the values of k obtained after 6 h are 0.0079 min^{-1} (r^2 = 0.992), 0.0050 min^{-1} (r^2 = 0.98) and 0.0022 min^{-1} (r^2 = 0.87), when ultrapure water, drinking water and secondary treated wastewater are used, respectively. It is noteworthy that the lower value of r^2 obtained with secondary treated wastewater reflects the higher complexity of this water matrix, making the experimental results harder to predict. Nevertheless, the decrease of SMX removal may be ascribed to the presence of (i) dissolved organic matter and/or (ii) radical scavengers in the more complex water matrices, especially in the secondary treated wastewater. Since HO• radicals are non-selective oxidants [17], the presence of organic matter is expected to limit the SMX removal; while, at the same time, ion species (e.g., bicarbonates, chlorides and sulphates) may act as HO• scavengers, as previously shown for photocatalytic applications [62]. In order to better understand how the CWPO process is influenced by each of these components, additional experiments were performed using humic acid (HA) to mimic the presence of dissolved organic matter, and sodium bicarbonate (500 mg L^{-1} bicarbonates), sodium chloride (200 mg L^{-1} chlorides) and sodium sulphate (60 mg L^{-1} sulphates) to mimic the presence of the typical inorganic constituents of conventionally treated wastewater and drinking water.

As observed in Fig. 10b, the SMX removal obtained in the experiment performed with a 10 mg L^{-1} HA solution remains nearly the same when compared to that obtained with ultrapure water. However, when bicarbonates (500 mg L^{-1}) are added to the 10 mg L^{-1} HA solution, the SMX removal is affected; in this case, the value of k obtained after 6 h is 0.0065 min^{-1} (r^2 = 0.992), which represents a ca. 16.7% decrease when compared to that obtained with ultrapure water. Therefore, it is possible to conclude that the removal of SMX by CWPO in the presence of CX/CoFe is affected by dissolved organic matter corresponding to a HA concentration of 10 mg L^{-1}, although in a small extent. Nevertheless, when the concentration of HA is increased up to 40 mg L^{-1} – i.e., an overestimated amount if the total organic carbon of the secondary treated wastewater used in this work is considered (6.2 mg L^{-1}) – the removal of SMX is greatly affected. Regarding the presence of inorganic species, it is observed that both bicarbonates, chlorides and sulphates have a negative impact on the removal of SMX by CWPO. Therefore, it is possible to conclude that the decrease of pollutant removal is mainly due to the presence of sulphates (30 mg L^{-1}) and organic matter (18.9 mg L^{-1} chemical oxygen demand), but it is also affected by chlorides (0.44 mg L^{-1}) and, possibly, by other unidentified constituents of the secondary treated wastewater considered. Regarding the drinking water employed, if the results shown in Fig. 10 are analysed

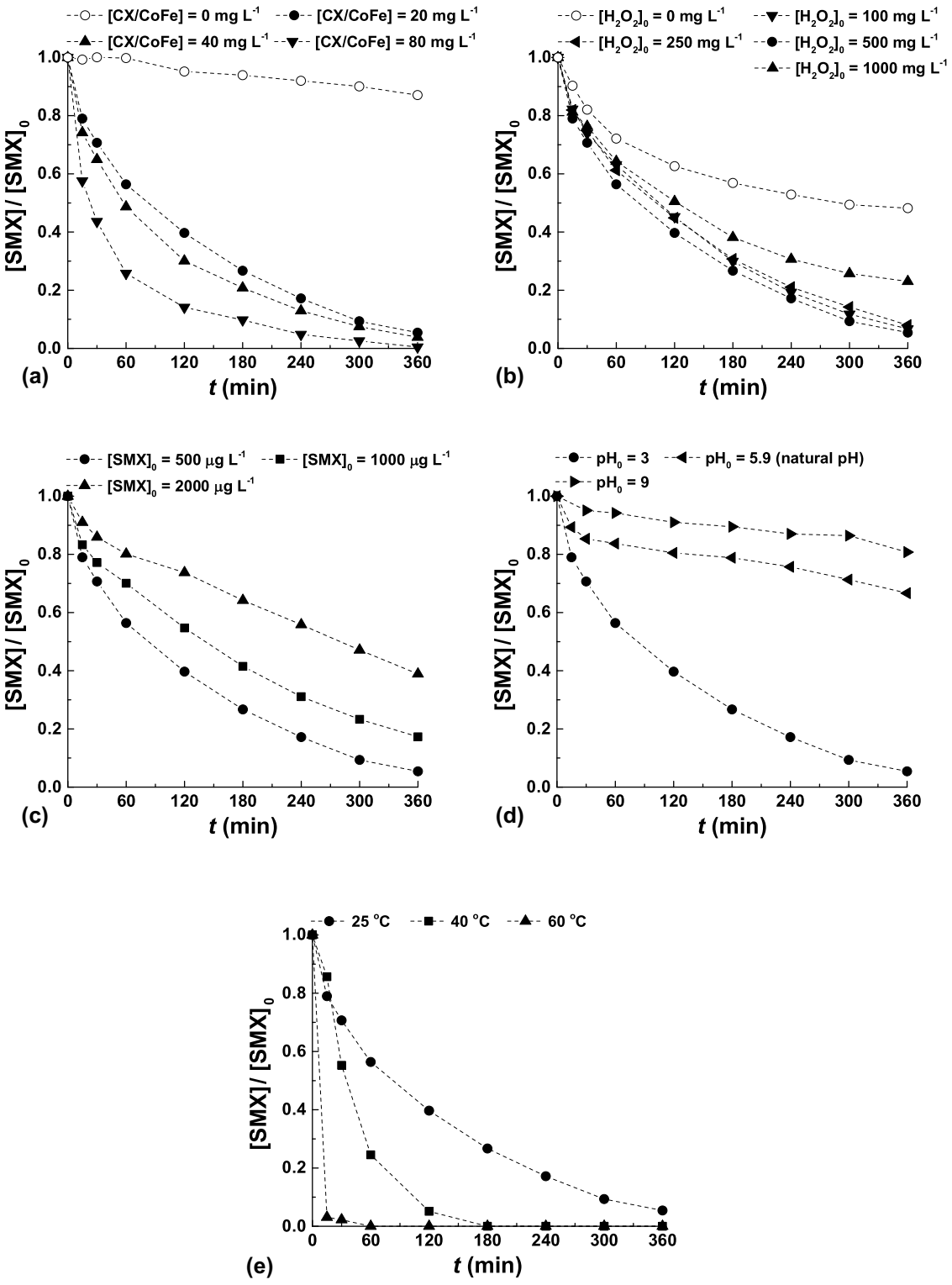

Fig. 8. Effect of (a) catalyst load, (b) $[H_2O_2]_0$, (c) $[SMX]_0$, (d) pH_o and (e) temperature, on the removal of SMX when using CX/CoFe.

together with the properties given in Section 2.2, it is possible to conclude that the removal of SMX in this water matrix is mainly affected by the presence of inorganic species, namely bicarbonates (211 mg L^{-1}), chlorides (9.8 mg L^{-1}) and sulphates (15 mg L^{-1}).

3.2.3. Reusability cycles

So far, the catalytic performance of CX/CoFe in the CWPO of SMX solutions was shown in different operating conditions and water matrices. Nevertheless, catalyst stability is also an essential requirement, especially for industrial/real-scale applications. Bearing this in mind, the catalyst stability of CX/CoFe in the CWPO of SMX was assessed through reusability cycles performed by implementation of a simple in-situ magnetic separation procedure for catalyst recovery and re-use, as depicted in Fig. 1. After the reaction stage, the treated water was recovered, and the catalyst reused in another CWPO run upon the addition of a fresh SMX solu-

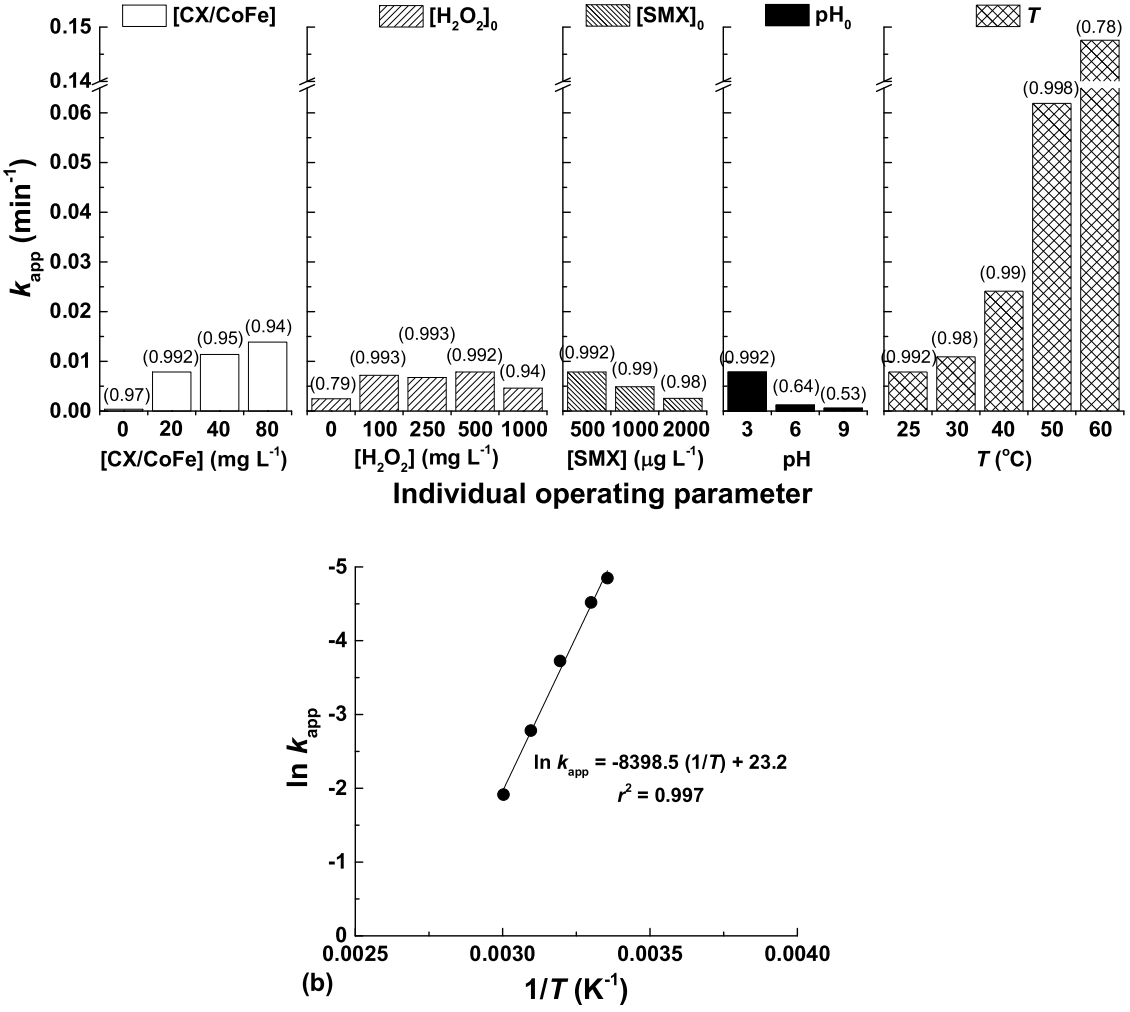

Fig. 9. (a) Apparent first order reaction rate constants (k_{app}) obtained after 6 h in experiments performed with CX/CoFe under different operating conditions. The numbers in brackets represent the regression coefficients of the linear fittings (r^2). (b) Arrhenius plot of the k_{app} values obtained at T = 25 °C, 30 °C, 40 °C, 50 °C and 60 °C.

tion (500 μg L^{-1}). In this way, the reusability cycles are able to mimic real-scale applications. As shown in Fig. 11, both ultrapure water and secondary treated wastewater were used in this study. However, based on the previous results, the catalyst dosage employed for the CWPO of SMX in secondary treated wastewater was increased 4-fold, up to 80 mg L^{-1}, in order to promote a SMX removal comparable to that obtained in ultrapure water.

As observed, the removal of SMX in the presence of CX/CoFe decreases in the two series of three consecutive CWPO runs. When ultrapure water is used, the SMX removal decreases from 94.6%, in the first run, to 64.6% and 51.4%, in the second and third runs, respectively. A higher decrease from the first to the second run is expected, due to the contribution of adsorption in the first use of CX/CoFe. As observed in Fig. 11b, this effect is more pronounced when secondary treated wastewater is employed, due to its higher complexity. Nevertheless, the ability of CWPO to eliminate SMX in secondary treated wastewater is unequivocally shown in Fig. 11b, with 96.8% of its initial content being removed after 6 h of reaction in the presence CX/CoFe (corresponding to k = 0.0102 min^{-1}; r^2 = 0.97). This achievement is even more relevant considering that the process was performed at room temperature and atmospheric pressure, thus opening a window of opportunity for the development of economically viable treatment options to reduce the propagation of SMX in the urban water cycles.

In order to better understand the deactivation phenomena responsible for the decrease of activity observed in consecutive CWPO cycles, the textural properties of the CX/CoFe recovered after the 1st CWPO cycle performed with SMX in ultrapure water were analysed by N_2 adsorption-desorption isotherms. It was found that the textural properties of CX/CoFe are not significantly affected by its application in the CWPO of SMX under the operating conditions considered. Specifically, only a ca. 2% decrease of the S_{BET} was observed (from 530 m^2 g^{-1} in the fresh catalyst, to 520 m^2 g^{-1} in the used catalyst). Since the textural properties of CX/CoFe were not significantly affected following the application in the CWPO of SMX, it is possible to conclude that the blockage of the porous structure is not the main cause of the catalyst deactivation. Bearing this in mind, thermogravimetric analysis (TGA) under oxidative atmosphere was used in order to better elucidate the causes of catalyst deactivation. It was found that the ash content of CX/CoFe slightly decreases upon its application in the CWPO of SMX (from 11.0 wt.% in the fresh catalyst, to 8.9 wt.% in the used catalyst, representing a ca. 2% decrease). This fact suggests that the leaching of active metal species may contribute to the catalyst deactivation observed. Nevertheless, it should be noted that the experimental procedure used during the CWPO reusability cycles may also affect the results obtained. Since no catalyst is added during the successive CWPO cycles, this more realistic approach may lead to a loss of catalyst mass caused by the periodical withdrawn of samples from the reactor (to analyse SMX concentration against time). Therefore, the catalyst deactivation may be slightly overestimated.

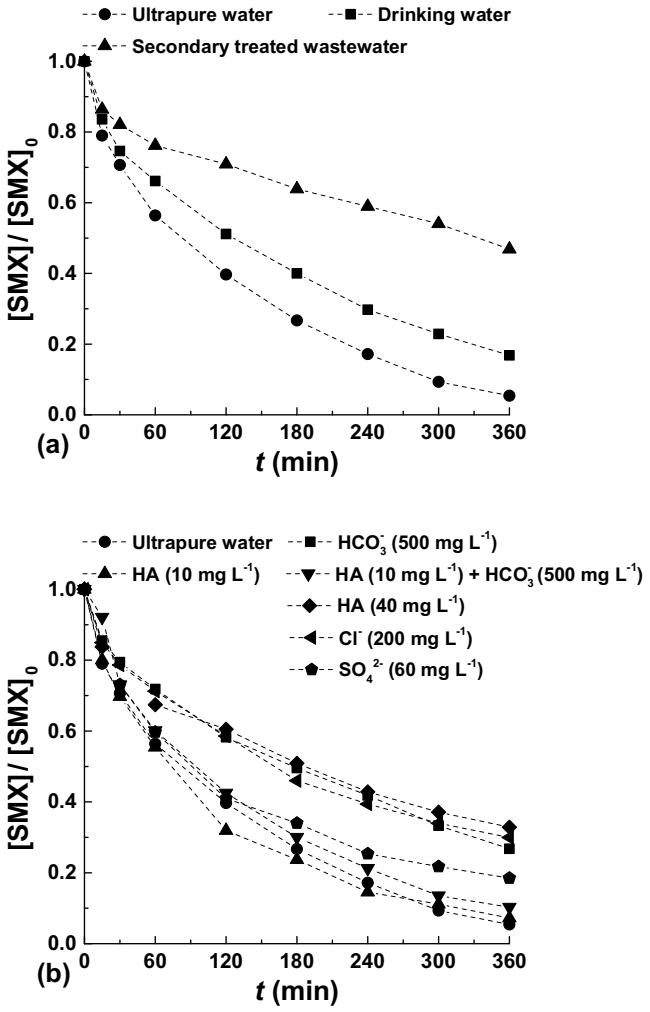

Fig. 10. Effect of (a) environmentally relevant and (b) synthetic water matrices on the CWPO removal of SMX when using CX/CoFe (20 mg L^{-1}) under the experimental conditions of Fig. 6.

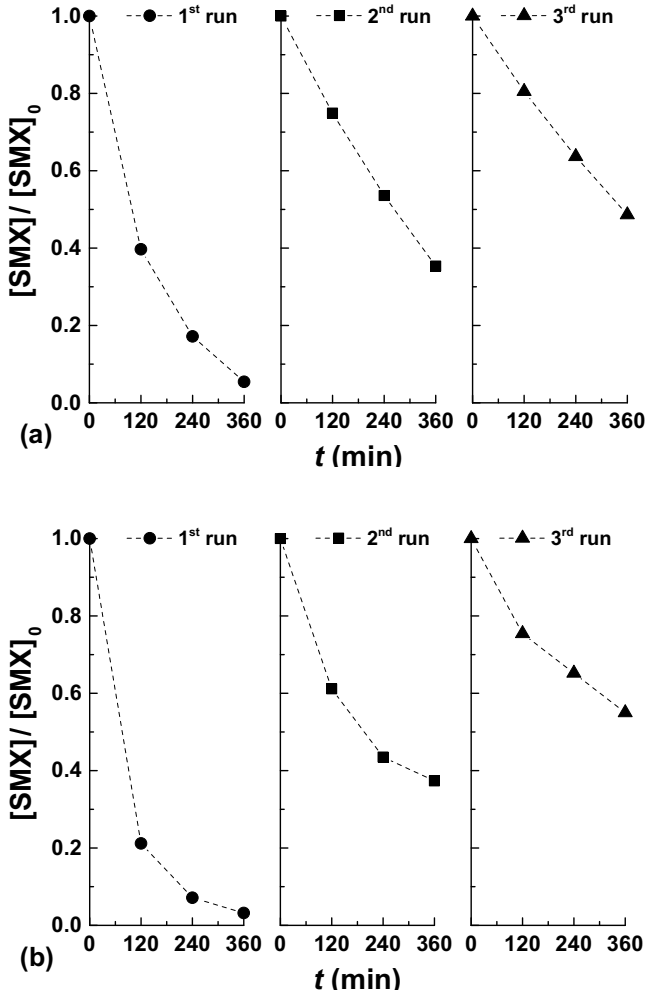

Fig. 11. Removal of SMX (500 μg L^{-1}) in (a) ultrapure water and (b) secondary treated wastewater, obtained in a series of three consecutive CWPO runs performed with CX/CoFe, as depicted in Fig. 1. Experiments performed at T = 25 °C, pH = 3, $[H_2O_2]_0$ = 500 mg L^{-1} and catalyst loads of (a) 20 mg L^{-1} and (b) 80 mg L^{-1}.

3.3. Antimicrobial activity and oxidation mechanism: a water treatment process intensification approach

The antibiotic activity of SMX was evaluated against two representative bacterial strains, namely *Klebsiella pneumoniae* (Gram negative) and *Staphylococcus aureus* (Gram positive). As observed in Fig. 12a, the antibiotic activity of SMX solutions at the ppb level (500 μg L^{-1}) is negligible for both the bacteria selected. However, when the concentration of SMX increases, the inherent antibiotic activity also increases. Regardless of the bacteria considered, 10 mg L^{-1} is the minimum SMX concentration that leads to a noticeable reduction of bacterial population (ca. 20–25%). Higher concentrations are more toxic, but less environmentally relevant. Therefore, a water treatment process intensification approach was used in order to evaluate the toxicity of the water prior and after treatment, considering 10 mg L^{-1} SMX solutions. In this way, although the study is performed at higher concentration than that occurring in environmentally relevant water matrices, the effects observed are amplified, and thus more accurate. In addition, it is possible to evaluate the mineralization levels obtained and to identify intermediates of SMX mineralization, allowing to propose a degradation mechanism for the CWPO of SMX in the presence of CX/CoFe.

Based on the knowledge gathered from the study performed on the individual effect of the operating parameters (cf. Section 3.2.1), the catalyst load was increased 10-fold and the H_2O_2 dosage 5-fold, although the SMX initial concentration was increased 20-fold. As observed in Fig. 12b, the kinetic constant of SMX removal (k = 0.0190 min^{-1}; r^2 = 0.991) is higher when compared to that previously shown in Fig. 7, regarding 500 μg L^{-1} SMX solutions (k = 0.0079 min^{-1}). These results are in accordance with recent findings on the higher efficiency of the CWPO process when the pollutant concentration is increased [39]. Under these conditions, ca. 42% TOC removal was obtained after 6 h of reaction, at the expenses of ca. 20% H_2O_2 consumption. Even in this water treatment process intensification approach, the leaching of Fe during the reaction was 1.2 mg L^{-1}, i.e., still in compliance with the common EU Directives for treated water to be discharged into natural receiving water bodies (2 mg L^{-1}); while the leaching of Co was 1.3 mg L^{-1}.

In order to assess the antimicrobial activity of the treated water, samples were collected during the reaction. As observed in Fig. 12, the antibiotic activity of the original SMX is lost upon oxidation; however, the treated water is more toxic to the particular microorganisms considered in this study. Specifically, a ca. 30% and 40% higher bacteria inhibition is observed when *S. aureus* and *K. pneumoniae* are considered, respectively. Since the toxicity of a mixture of pharmaceutical drugs is usually higher than that of the sum of each individual compound [63], the overall toxicity of the treated water is expected to increase as new byproducts are formed. Actually, this effect is very common in photocatalytic applications [2].

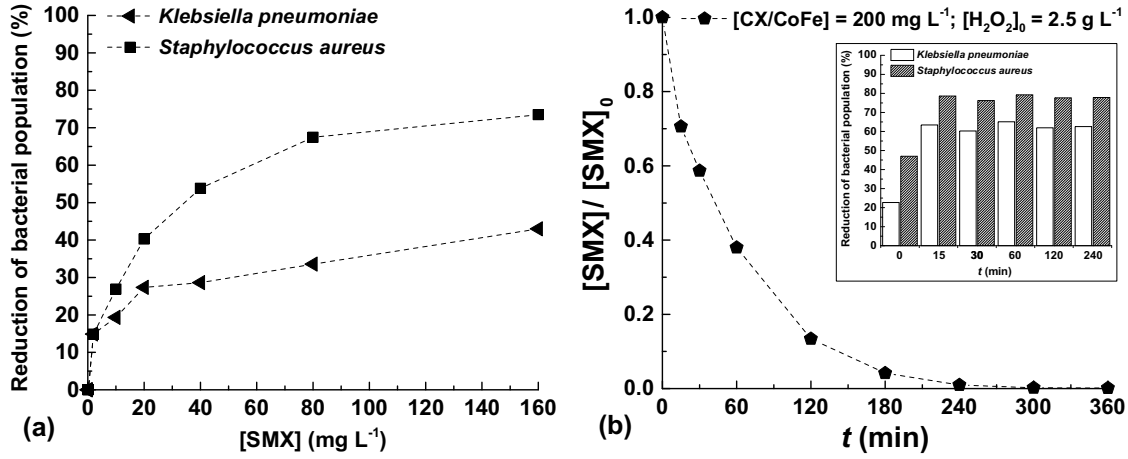

Fig. 12. Reduction of bacterial population (a) as a function of SMX concentration and (b) during the CWPO removal of SMX when using CX/CoFe under intensified conditions (10 mg L^{-1}).

Table 3
High resolution accurate mass data (retention time (R_t), pseudo-molecular ion formula, $[M+H]^+$, $[M+Na]^+$, relative error Δ (ppm) and ring-double bond equivalents (RDBE)) for SMX and TBPs in positive ionization mode.

TBP code	R_t (min)	Pseudo-molecular ion formula	m/z $[M+H]^+/[M+Na]^+$	Δ (ppm)	RDBE
TBP1	1.5	$C_6H_8NO_3S$	174.0216	1.8	3.5
TBP2	4.5	$C_{10}H_{14}N_3O_5S$	288.0659	−3.4	5.5
TBP3	4.7	$C_7H_{10}N_3O_3S$	216.0453	−7.2	4.5
TBP4	5.3	$C_{10}H_{12}N_3O_4S$	270.0552	−3.4	6.5
TBP5	5.6	$C_{10}H_{14}N_3O_4S$	272.0700	−0.2	5.5
TBP6	6.1	$C_{10}H_{12}N_3O_4S$	270.0562	−7.1	6.5
SMX[a]	8.1	$C_{10}H_{12}N_3O_3S$	254.0589	2.0	6.5
		$C_{10}H_{11}N_3NaO_3S$	276.0404	3.5	
TBP7	8.8	$C_9H_{10}N_3O_7S$	304.0235	−0.4	6.5
TBP8	8.9	$C_{10}H_{10}N_3O_5S$	284.0335	0.2	7.5
		$C_{10}H_9N_3NaO_5S$	306.0149	2.1	
TBP9	9.2	$C_{10}H_{10}N_3O_6S$	300.0290	−1.8	7.5
TBP10[a]	10.6	$C_{10}H_{10}N_3O_6S$	300.0274	3.6	7.5
		$C_{10}H_9N_3NaO_5S$	322.0093	3.6	
TBP11[a]	10.8	$C_{10}H_{10}N_3O_5S$	284.0322	4.7	7.5
		$C_{10}H_9N_3NaO_5S$	306.0141	4.7	

[a] TBPs detected in both positive and negative ionization mode.

Table 4
High resolution accurate mass data (retention time (R_t), pseudo-molecular ion formula, $[M-H]^-$, relative error Δ (ppm) and ring-double bond equivalents (RDBE)) for SMX and TBPs in negative ionization mode.

TBP code	R_t (min)	Pseudo-molecular ion formula	m/z $[M-H]^-$	Δ (ppm)	RDBE
TBP12	3.7	$C_4H_5N_2O_4S$	176.9981	−3.2	3.5
TBP13	6.6	$C_6H_4NO_5S$	201.9816	0	5.5
SMX[a]	8.1	$C_{10}H_{10}N_3O_3S$	252.0452	−1.4	7.5
TBP10[a]	10.6	$C_{10}H_8N_3O_6S$	298.0133	2.0	8.5
TBP11[a]	10.8	$C_{10}H_8N_3O_5S$	282.0181	3.1	8.5
		$C_6H_4NO_4S$	185.9878	−6.1	5.5

[a] TBPs detected in both positive and negative ionization mode.

Nevertheless, the intermediates of SMX mineralization obtained by CWPO were identified in order to get further insights on this regard. Samples collected at 0, 15, 30, 60, 120, 240 and 360 min of reaction were analyzed by LC-TOF-MS in both positive and negative ionization mode. The majority of the TBPs were identified under positive ionization mode. The pseudo-molecular ions, retention time, the corresponding molecular formulas proposed, the relative mass error and the RDBE (Ring Double Bond Equivalents) for the 13 TBPs identified under the adopted conditions are compiled in Tables 3 and 4. Based on the TBPs identified through this approach, the major degradation pathways for the CWPO of SMX were determined, as given in Fig. 13.

A first pathway initiated by the $HO^•$ radical attack on the SMX molecule includes the hydroxylation of either phenyl and/or isoxazole rings and the formation of two hydroxylated TBPs (TBP4 and TBP6). Regarding the possible hydroxylation of phenyl ring and due to the electron-donating effect of $-NH_2$ and the electron-withdrawing effect of $-S(O_2)-NH-$ groups the formation of the *ortho*-derivative relative to the $-NH_2$ group can be expected. Similarly, in the case of electrochemical treatment of sulfachloropyridazine antibiotic which also bears a sulfanilinic moiety, the *ortho*-hydroxylated derivative was proposed [64]. A parallel hydroxylation route proceeds through the $HO^•$ attack to the double bond on the isoxazole ring and the formation of TBP5 and TBP2, in agreement with the reduction in the RDBE value (Table 3). The formation of TBP2 has been identified in accordance to the mechanism proposed by Hu et al. [65]. The mechanism involves a tertiary carbon-centered radical formed from the $HO^•$ radical

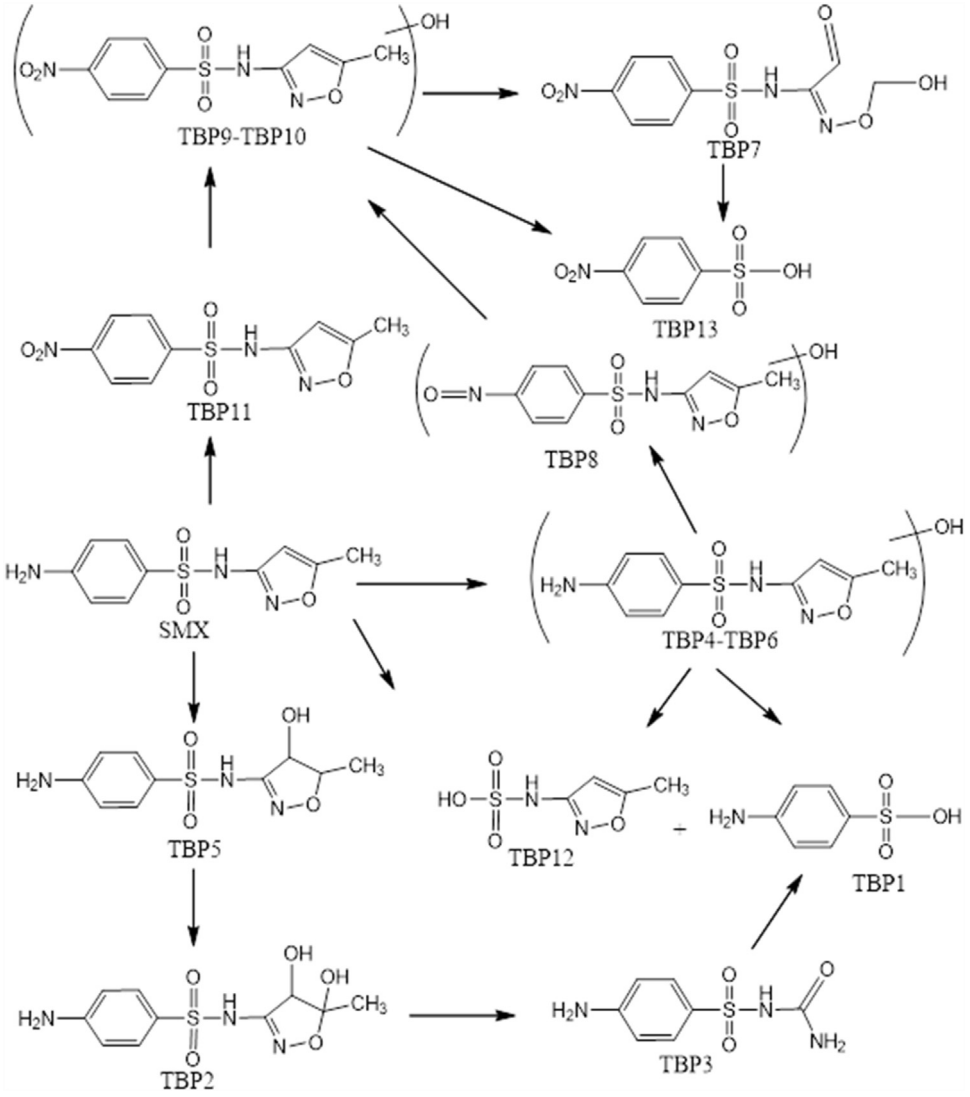

Fig. 13. Proposed degradation pathway for the CWPO of SMX.

attack and the subsequent addition of dissolved oxygen resulting in the corresponding peroxy radical and hydroperoxide followed by the homolytical cleavage of hydroperoxide [65]. On its turn, TBP2 further gives rise to TBP3 via the successive isoxazole ring opening. Hydroxylation is a well-reported pathway during the degradation of SMX by various AOP. Similar hydroxy-TBPs have been previously described as by-products of TiO_2 photocatalysis, photo-Fenton, ultrasound/ozone oxidation, ferrous-activated persulfate oxidation, thermo activated persulfate oxidation, ozonation, catalytic ozonation and electrochemical oxidation, among others [65–73].

The second pathway, which can be characterized as the major route based on the area of the identified TBPs, is assigned to the oxidation of the amino group of the benzene ring yielding the formation of the nitro-derivative of SMX (TBP11). This oxidation pathway has also been reported previously during the degradation of SMX using ultrasound/ozone oxidation system [68], Co(II)/PMS system [74], thermo activated persulfate oxidation [70] and other AOP with different oxidants such as ferrate [75], chlorine, ozone and permanganate [76]. The formation of nitro-derivative is rationalized through the formation of hydroxylamine as a result of $HO^{\bullet}$ radical attack on the $-NH_2$ group, followed by the formation of nitroso derivatives which are readily transformed into nitro-SMX [74]. The TBP11 is also subjected to hydroxylation (TBP9, TBP10), followed by isoxazole ring opening (TBP7) and progressive oxidation/decarboxylation or cleavage of sulfonamide bond to form TBP13. TBPs derived from the oxidation of the amino group at the benzene ring and cleavage of the isoxazole ring have also been identified in ultrasound/ozone oxidation process by Guo et al. [68]. Furthermore, oxidation of amino group of the hydroxy-TBPs leads to the formation of the hydroxylated nitroso- derivative (TBP8). This TBP has been reported during ozonation [71] and catalytic ozonation [66] of SMX.

A third degradation pathway initiated by $HO^{\bullet}$ radical attack proceeds through sulfonamide (S—N) bond and C—S cleavages, yielding the formation of 4-amino-benzene-sulfonic acid (TBP1) and 5-methylisoxazol-3-ylsulfamic acid (TBP12). The cleavage of sulfonamide bond has been widely observed in the oxidation of SMX by other AOP [65,67,74–77]. Subsequent oxidation steps of the identified TBPs results in the opening of the benzoic and isoxazole rings and the progressive formation of lower molecular weight organic compounds such as aliphatic alcohols, aldehydes, and carboxylic acids [65,66], in accordance with the partial mineralization observed (ca. 42% TOC removal).

The possible bactericidal effect of Fe and Co leached to the treated water during the CWPO of SMX in the presence of CX/CoFe

was also assessed. Accordingly, a set of experiments was performed in the dark with 2.0 mg L^{-1} Fe and Co solutions spiked with the bacteria of interest (i.e., *K. pneumoniae* and *S. aureus*), as described in Section 2.7. It was found that both metal ions do not exhibit any biocidal activity and no induced stress was observed in the cells after their exposure.

4. Conclusions

A clear synergistic effect arises from the simultaneous incorporation of Co and Fe in the magnetic carbon xerogel material denoted as CX/CoFe, when its performance in the CWPO of SMX at the ppb level (500 μg L^{-1}) is compared to that of monometallic catalysts containing only Fe or Co. This effect was ascribed to the higher accessibility of Fe species promoted by the simultaneous incorporation of Co.

As a result of its improved performance, CX/CoFe is able to promote an effective CWPO removal of SMX from secondary treated wastewater, the degradation of SMX proceeding via three main pathways: (i) oxidation of the amine group to yield the nitro TBPs, (ii) hydroxylation of the benzene and isoxazole rings, and (iii) cleavage of the sulfonamide bond. This feature opens future prospects for the development of economically viable CWPO-based technologies able to reduce the propagation of SMX in urban water cycles. However, further studies should comprise eco-toxicity evaluations in real scenario applications, in which several micropollutants are present at trace concentrations rather than only one pollutant at higher concentration than that occurring in the urban water cycles.

Acknowledgments

This work was financially supported by: Project POCI-01-0145-FEDER-006984 – Associate Laboratory LSRE-LCM funded by FEDER through COMPETE2020 – Programa Operacional Competitividade e Internacionalização (POCI) – and by national funds through FCT – Fundaçã opara a Ciência e a Tecnologia. R.S. Ribeiro acknowledges the FCT individual Ph.D. grant SFRH/BD/94177/2013, with financing from FCT and the European Social Fund (through POPH and QREN). A.M.T. Silva acknowledges the FCT Investigator 2013 Programme (IF/01501/2013), with financing from the European Social Fund and the Human Potential Operational Programme.

The authors also would like to acknowledge the financial support provided by COST-European Cooperation in Science and Technology, to the COST Action ES1403: New and emerging challenges and opportunities in wastewater reuse (NEREUS).

Disclaimer

The content of this article is the authors' responsibility and neither COST nor any person acting on its behalf is responsible for the use, which might be made of the information contained in it.

References

[1] I. Michael-Kordatou, C. Michael, X. Duan, X. He, D.D. Dionysiou, M.A. Mills, D. Fatta-Kassinos, Water Res. 77 (2015) 213–248.
[2] D. Fatta-Kassinos, S. Meric, A. Nikolaou, Anal. Bioanal. Chem. 399 (2011) 251–275.
[3] L. Rizzo, C. Manaia, C. Merlin, T. Schwartz, C. Dagot, M.C. Ploy, I. Michael, D. Fatta-Kassinos, Sci. Total Environ. 447 (2013) 345–360.
[4] M.F. Ferreira da Silva, I. Tiago, A. Veríssimo, R.A.R. Boaventura, O.C. Nunes, C.M. Manaia, FEMS Microbiol. Ecol. 55 (2006) 322–329.
[5] V. Figueira, E. Serra, C.M. Manaia, Sci. Total Environ. 409 (2011) 1017–1023.
[6] K. Kümmerer, Chemosphere 75 (2009) 435–441.
[7] A. Lupo, S. Coyne, T.U. Berendonk, Front. Microbiol. 3 (2012) 18.
[8] M.O. Barbosa, N.F.F. Moreira, A.R. Ribeiro, M.F.R. Pereira, A.M.T. Silva, Water Res. 94 (2016) 257–279.
[9] A.R. Ribeiro, O.C. Nunes, M.F.R. Pereira, A.M.T. Silva, Environ. Int. 75 (2015) 33–51.
[10] The White House, National strategy for combating antibiotic-resistant bacteria, Washington, US (2014).
[11] D. Fatta-Kassinos, C. Manaia, T.U. Berendonk, E. Cytryn, J. Bayona, B. Chefetz, J. Slobodnik, N. Kreuzinger, L. Rizzo, S. Malato, L. Lundy, A. Ledin, Environ. Sci. Pollut. Res. 22 (2015) 7183–7186.
[12] Y. Luo, W. Guo, H.H. Ngo, L.D. Nghiem, F.I. Hai, J. Zhang, S. Liang, X.C. Wang, Sci. Total Environ. 473–474 (2014) 619–641.
[13] W.H. Glaze, J.-W. Kang, D.H. Chapin, Ozone Sci. Eng. 9 (1987) 335–352.
[14] C.W. Jones, Applications of Hydrogen Peroxide and Derivatives, The Royal Society of Chemistry, Cambridge, UK, 1999.
[15] J.J. Pignatello, E. Oliveros, A. MacKay, Crit. Rev. Environ. Sci. Technol. 36 (2006) 1–84.
[16] P.R. Gogate, A.B. Pandit, Adv. Environ. Res. 8 (2004) 501–551.
[17] S. Navalon, M. Alvaro, H. Garcia, Appl. Catal. B 99 (2010) 1–26.
[18] F. Haber, J. Weiss, Proc. R. Soc. Lond. A Math. Phys. Sci. 147 (1934) 332–351.
[19] H.J.H. Fenton, J. Chem. Soc. Trans. 65 (1894) 899–910.
[20] J.A. Zazo, J.A. Casas, A.F. Mohedano, J.J. Rodríguez, Appl. Catal. B 65 (2006) 261–268.
[21] M.C. Pereira, L.C.A. Oliveira, E. Murad, Clay Miner. 47 (2012) 285–302.
[22] M. Munoz, Z.M. de Pedro, J.A. Casas, J.J. Rodriguez, Appl. Catal. B 176–177 (2015) 249–265.
[23] P.V. Nidheesh, RSC Adv. 5 (2015) 40552–40577.
[24] S. Rahim Pouran, A.A. Abdul Raman, W.M.A. Wan Daud, J. Clean. Prod. 64 (2014) 24–35.
[25] M. Muruganandham, R.P.S. Suri, M. Sillanpää, J.J. Wu, B. Ahmmad, S. Balachandran, M. Swaminathan, J. Nanosci. Nanotechnol. 14 (2014) 1898–1910.
[26] A. Dhakshinamoorthy, S. Navalon, M. Alvaro, H. Garcia, ChemSusChem 5 (2012) 46–64.
[27] S. Navalon, A. Dhakshinamoorthy, M. Alvaro, H. Garcia, ChemSusChem 4 (2011) 1712–1730.
[28] S. Navalon, R. Martin, M. Alvaro, H. Garcia, Angew. Chem. Int. Ed. 49 (2010) 8403–8407.
[29] J.H. Ramirez, F.J. Maldonado-Hódar, A.F. Pérez-Cadenas, C. Moreno-Castilla, C.A. Costa, L.M. Madeira, Appl. Catal. B 75 (2007) 312–323.
[30] A. Rodríguez, G. Ovejero, J.L. Sotelo, M. Mestanza, J. García, Ind. Eng. Chem. Res. 49 (2010) 498–505.
[31] L.C.A. Oliveira, C.N. Silva, M.I. Yoshida, R.M. Lago, Carbon 42 (2004) 2279–2284.
[32] F. Lücking, H. Köser, M. Jank, A. Ritter, Water Res. 32 (1998) 2607–2614.
[33] Q. Liao, J. Sun, L. Gao, Colloids Surf. A 345 (2009) 95–100.
[34] C.M. Domínguez, A. Quintanilla, P. Ocón, J.A. Casas, J.J. Rodríguez, Carbon 60 (2013) 76–83.
[35] F.M. Duarte, F.J. Maldonado-Hódar, A.F. Pérez-Cadenas, L.M. Madeira, Appl. Catal. B 85 (2009) 139–147.
[36] R.S. Ribeiro, N.A. Fathy, A.A. Attia, A.M.T. Silva, J.L. Faria, H.T. Gomes, Chem. Eng. J. 195–196 (2012) 112–121.
[37] R.S. Ribeiro, A.M.T. Silva, M.T. Pinho, J.L. Figueiredo, J.L. Faria, H.T. Gomes, Catal. Today 240 (Part A) (2015) 61–66.
[38] R.S. Ribeiro, A.M.T. Silva, L.M. Pastrana-Martínez, J.L. Figueiredo, J.L. Faria, H.T. Gomes, Catal. Today 249 (2015) 204–212.
[39] R.S. Ribeiro, A.M.T. Silva, J.L. Figueiredo, J.L. Faria, H.T. Gomes, Appl. Catal. B 187 (2016) 428–460.
[40] J. Chaichanawong, T. Yamamoto, S.-I. Kim, T. Ohmori, J. Non Cryst. Solids 355 (2009) 1605–1612.
[41] X. Wang, X. Wang, L. Liu, L. Bai, H. An, L. Zheng, L. Yi, J. Non Cryst. Solids 357 (2011) 793–797.
[42] J. Benner, D.E. Helbling, H.-P.E. Kohler, J. Wittebol, E. Kaiser, C. Prasse, T.A. Ternes, C.N. Albers, J. Aamand, B. Horemans, D. Springael, E. Walravens, N. Boon, Water Res. 47 (2013) 5955–5976.
[43] H.T. Gomes, B.F. Machado, A. Ribeiro, I. Moreira, M. Rosário, A.M.T. Silva, J.L. Figueiredo, J.L. Faria, J. Hazard. Mater. 159 (2008) 420–426.
[44] Y. Wang, H. Zhao, G. Zhao, Appl. Catal. B 164 (2015) 396–406.
[45] S. Brunauer, P.H. Emmett, E. Teller, J. Am. Chem. Soc. 60 (1938) 309–319.
[46] F. Rodríguez-Reinoso, A. Linares-Solano, Physics of Carbon, Marcel Dekker Inc., New York, 1989.
[47] M. Thommes, K. Kaneko, A.V. Neimark, J.P. Olivier, F. Rodriguez-Reinoso, J. Rouquerol, K.S.W. Sing, Pure Appl. Chem. 87 (2015) 1051–1069.
[48] S. Lowell, J.E. Shields, M.A. Thomas, M. Thommes, Characterization of Porous Solids and Powders: Surface Area, Pore Size and Density, Springer Science + Business Media, New York, 2004.
[49] L.M. Pastrana-Martínez, S. Morales-Torres, S.K. Papageorgiou, F.K. Katsaros, G.E. Romanos, J.L. Figueiredo, J.L. Faria, P. Falaras, A.M.T. Silva, Appl. Catal. B 142–143 (2013) 101–111.
[50] M.A. Ferro-García, J. Rivera-Utrilla, I. Bautista-Toledo, C. Moreno-Castilla, Langmuir 14 (1998) 1880–1886.
[51] J. Rivera-Utrilla, I. Bautista-Toledo, M.A. Ferro-García, C. Moreno-Castilla, J. Chem. Technol. Biotechnol. 76 (2001) 1209–1215.
[52] A. Rey, A. Bahamonde, J.A. Casas, J.J. Rodríguez, Water Sci. Technol. 61 (2010) 2769–2778.
[53] R.S. Ribeiro, A.M.T. Silva, J.L. Figueiredo, J.L. Faria, H.T. Gomes, Carbon 62 (2013) 97–108.
[54] ISO 6332:1988, Water quality – Determination of iron – Spectrometric method using 1,10-phenanthroline, International Organization for Standardization (1988).

[55] J.H. Ramirez, C.A. Costa, L.M. Madeira, G. Mata, M.A. Vicente, M.L. Rojas-Cervantes, A.J. López-Peinado, R.M. Martín-Aranda, Appl. Catal. B 71 (2007) 44–56.
[56] C. Moreno-Castilla, F.J. Maldonado-Hodar, Carbon 43 (2005) 455–465.
[57] M. Kosmulski, J. Colloid Interface Sci. 426 (2014) 209–212.
[58] Council Directive 98/83/EC of 3 November 1998 on the quality of water intended for human consumption, Official Journal of the European Communities, The Council of the European Union (1998).
[59] E.P. Agency, Parameters of Water Quality: Interpretation and Standards, Environmental Protection Agency, Ireland, Wexford Ireland, 2001.
[60] N. Inchaurrondo, J.O. Cechini, J. Font, P. Haure, Appl. Catal. B 111–112 (2012) 641–648.
[61] D. Dimitrakopoulou, I. Rethemiotaki, Z. Frontistis, N.P. Xekoukoulotakis, D. Venieri, D. Mantzavinos, J. Environ. Manag. 98 (2012) 168–174.
[62] O. Tsydenova, V. Batoev, A. Batoeva, Int. J. Environ. Res. Public Health 12 (2015) 9542–9561.
[63] EEA, Pharmaceuticals in the environment, European Environment Agency, Copenhagen (2010).
[64] A. Dirany, I. Sirés, N. Oturan, A. Özcan, M.A. Oturan, Environ. Sci. Technol. 46 (2012) 4074–4082.
[65] L. Hu, P.M. Flanders, P.L. Miller, T.J. Strathmann, Water Res. 41 (2007) 2612–2626.
[66] D. Shahidi, A. Moheb, R. Abbas, S. Larouk, R. Roy, A. Azzouz, J. Hazard. Mater. 298 (2015) 338–350.
[67] A.G. Trovó, R.F.P. Nogueira, A. Agüera, A.R. Fernandez-Alba, C. Sirtori, S. Malato, Water Res. 43 (2009) 3922–3931.
[68] W.-Q. Guo, R.-L. Yin, X.-J. Zhou, J.-S. Du, H.-O. Cao, S.-S. Yang, N.-Q. Ren, Ultrason. Sonochem. 22 (2015) 182–187.
[69] Y. Ji, C. Ferronato, A. Salvador, X. Yang, J.-M. Chovelon, Sci. Total Environ. 472 (2014) 800–808.
[70] Y. Ji, Y. Fan, K. Liu, D. Kong, J. Lu, Water Res. 87 (2015) 1–9.
[71] M.d.M. Gómez-Ramos, M. Mezcua, A. Agüera, A.R. Fernández-Alba, S. Gonzalo, A. Rodríguez, R. Rosal, J. Hazard. Mater. 192 (2011) 18–25.
[72] S. Hussain, S. Gul, J.R. Steter, D.W. Miwa, A.J. Motheo, Environ. Sci. Pollut. Res. 22 (2015) 15004–15015.
[73] M.N. Abellán, B. Bayarri, J. Giménez, J. Costa, Appl. Catal. B 74 (2007) 233–241.
[74] M. Mahdi Ahmed, S. Barbati, P. Doumenq, S. Chiron, Chem. Eng. J. 197 (2012) 440–447.
[75] V.K. Sharma, S.K. Mishra, N. Nesnas, Environ. Sci. Technol. 40 (2006) 7222–7227.
[76] S. Gao, Z. Zhao, Y. Xu, J. Tian, H. Qi, W. Lin, F. Cui, J. Hazard. Mater. 274 (2014) 258–269.
[77] A.G. Gonçalves, J.J.M. Órfão, M.F.R. Pereira, J. Hazard. Mater. 239–240 (2012) 167–174.